Discovery of two distinct aminoacyl-tRNA synthetase complexes anchored to the Plasmodium surface tRNA import protein

José Refugio Jaramillo Ponce, Delphine Kapps, Caroline Paulus, Johana Chicher, Magali Frugier

Discovery of two distinct aminoacyl-tRNA synthetase complexes anchored to the *Plasmodium* surface tRNA import protein

Received for publication, December 20, 2021, and in revised form, April 19, 2022 Published, Papers in Press, April 27, 2022,
https://doi.org/10.1016/j.jbc.2022.101987

José R. Jaramillo Ponce[1], Delphine Kapps[1], Caroline Paulus[1], Johana Chicher[2], and Magali Frugier[1,*]

From the [1]Université de Strasbourg, CNRS, Architecture et Réactivité de l'ARN, UPR 9002, Strasbourg, France; [2]Strasbourg-Esplanade Proteomics Facility, Université de Strasbourg, Strasbourg, France

Edited by Karin Musier-Forsyth

Aminoacyl-tRNA synthetases (aaRSs) attach amino acids to their cognate transfer RNAs. In eukaryotes, a subset of cytosolic aaRSs is organized into a multisynthetase complex (MSC), along with specialized scaffolding proteins referred to as aaRS-interacting multifunctional proteins (AIMPs). In *Plasmodium*, the causative agent of malaria, the tRNA import protein (tRip), is a membrane protein that participates in tRNA trafficking; we show that tRip also functions as an AIMP. We identified three aaRSs, the glutamyl-tRNA synthetase (ERS), glutaminyl-tRNA synthetase (QRS), and methionyl-tRNA synthetase (MRS), which were specifically coimmunoprecipitated with tRip in *Plasmodium berghei* blood stage parasites. All four proteins contain an N-terminal glutathione-*S*-transferase (GST)–like domain that was demonstrated to be involved in MSC assembly. In contrast to previous studies, further dissection of GST-like interactions identified two exclusive heterotrimeric complexes: the Q-complex (tRip–ERS–QRS) and the M-complex (tRip–ERS–MRS). Gel filtration and light scattering suggest a 2:2:2 stoichiometry for both complexes but with distinct biophysical properties and mutational analysis further revealed that the GST-like domains of QRS and MRS use different strategies to bind ERS. Taken together, our results demonstrate that neither the singular homodimerization of tRip nor its localization in the parasite plasma membrane prevents the formation of MSCs in *Plasmodium*. Besides, the extracellular localization of the tRNA-binding module of tRip is compensated by the presence of additional tRNA-binding modules fused to MRS and QRS, providing each MSC with two spatially distinct functions: aminoacylation of intraparasitic tRNAs and binding of extracellular tRNAs. This unique host–pathogen interaction is discussed.

Aminoacyl-tRNA synthetases (aaRSs) are a family of essential enzymes that perform the first step in protein synthesis by specifically attaching an amino acid to its corresponding tRNA (1). In addition to their canonical role in tRNA aminoacylation, eukaryotic aaRSs have evolved to participate in a wide range of alternative functions (2, 3). These functions include regulation of gene expression, RNA processing and trafficking, as well as cell signaling activities (4, 5). In eukaryotes, the association of several aaRSs within a multi-aaRS complex (MSC) partitions the translational activities of aaRSs while in the MSC, from their alternative functions once dissociated from the MSC (6–8). In addition to a subset of cytosolic aaRSs, MSCs contain up to three accessory proteins referred as aaRS-interacting multifunctional proteins (AIMPs) (Fig. 1*A*) (reviewed in (9, 10)). One AIMP is common to all known MSCs. In unicellular eukaryotes, it is a single polypeptide characterized by a specific structural organization: an N-terminal domain with homology to glutathione transferases (glutathione-*S*-transferase [GST]–like domain) fused through a poly-lysine linker to a C-terminal endothelial monocyte-activating polypeptide II (EMAPII)–like domain (11, 12) (Fig. 1*A*). GST-like domains are known to mediate protein–protein interactions, while EMAPII-like domains have been shown to recognize the tRNA 3D structure. This AIMP was first identified in the yeast *Saccharomyces cerevisiae* (Arc1p (13)) and in pathogenic parasites like *Toxoplasma gondii* (Tg43 (14)) and *Trypanosoma brucei* (MCP1 (15)). In metazoans, it is assembled from two separate peptides, either AIMP1 (p43, EMAPII-like domain) and AIMP2 (p38, GST-like domain) in vertebrates (16) or the C-terminal domain (EMAPII-like domain) of the methionyl-tRNA synthetase (MRS) and AIMP2 in nematodes (17). The bifunctional organization of these AIMPs (tRNA binding and protein–protein interaction domains) is crucial for MSCs to participate in tRNA channeling (18–20), subcellular location of aaRSs to control their noncanonical functions (21–23), and cellular turnover, by protecting associated proteins from degradation (24).

The sizes and compositions of MSCs vary among organisms and usually reflect their biological complexities (25) (Fig. 1*B*). However, despite their diversity, MSC assembly follows a common strategy involving GST-like modules found exclusively in eukaryotic aaRSs, AIMPs, and elongation factors EF1Bγ and EF1Bβ (10, 26–29). For instance, the yeast MSC is a trimer where the GST-like domains of MRS, glutamyl-tRNA synthetase (ERS) and Arc1p associate (30). In *T. gondii*, the MSC is composed of Tg-p43 and four aaRSs, MRS, ERS, glutaminyl-tRNA synthetase (QRS), and tyrosyl-tRNA synthetase (YRS) ,

* For correspondence: Magali Frugier, m.frugier@ibmc-cnrs.unistra.fr.

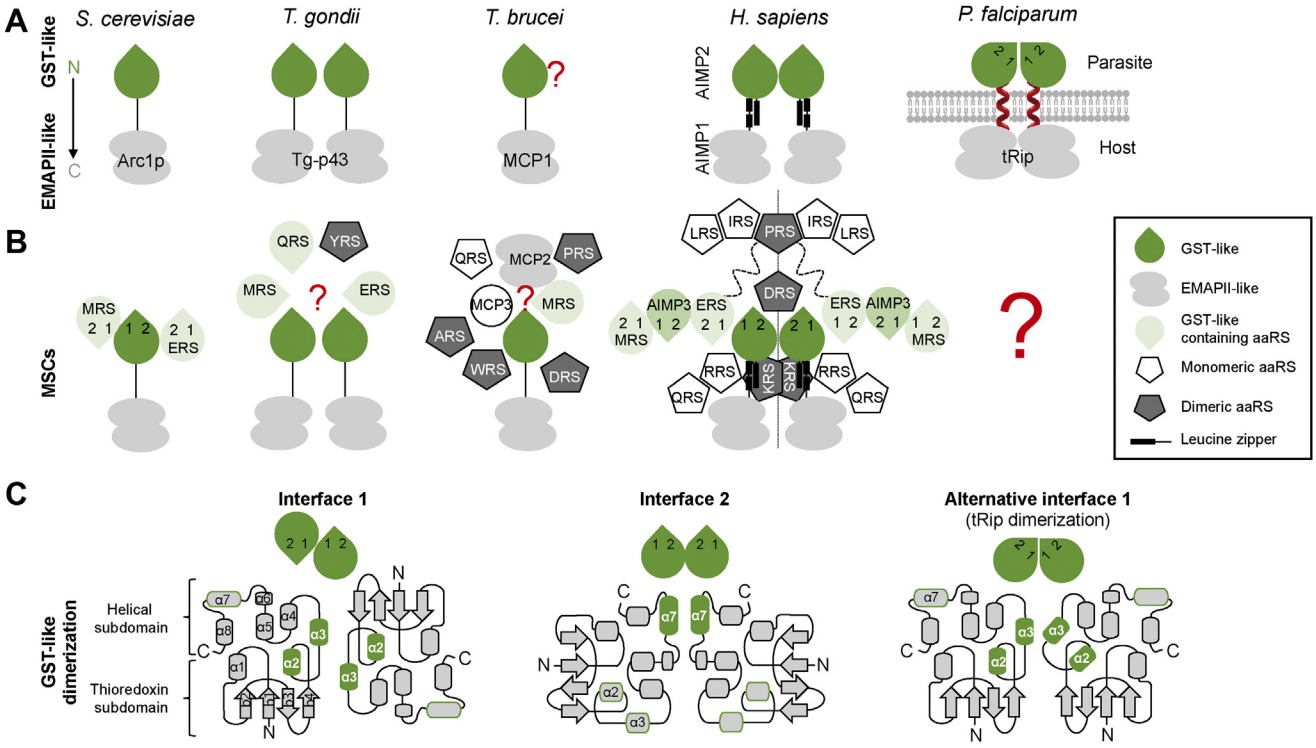

Figure 1. Structural diversity of eukaryotic MSCs. *A*, variability in proteins containing N-terminal GST and C-terminal EMAPII-like domains. *S. cerevisiae* Arc1p is monomeric (30, 54), *T. gondii* Tg-p43 is dimeric (14) and nothing is known about the oligomerization of *T. brucei* MCP1 (15). The interactions between the two leucine-zippers of human AIMP1 and AIMP2 reconstitute a split protein with the same topology as Tg-p43 since it can homodimerize *via* the GST domain of AIMP2 (84). All of them are cytosolic while the plasmodial protein, tRip, is a dimer and is localized to the plasma membrane (43). *B*, MSC architectures. In *S. cerevisiae*, Arc1p binds to ERS and MRS and MSC assembly occurs only *via* GST-like domains (39). The *T. gondii* MSC is composed of Tg-p43 and four aaRSs: ERS, QRS, MRS, and YRS, where only YRS lacks a GST-like domain. *T. brucei* MSC contains three AIMPs (MCP1, MCP2, and MCP3) and at least six aaRSs (QRS, ARS, WRS, PRS, DRS, and MRS). Among these aaRSs, only MRS contains a GST-like domain. How the proteins associate in these two parasite MSCs is still unknown (indicated by *red question mark*). In the human MSC, AIMP2 is the component with the largest number of binding partners and is essential for complex assembly. Human MSC components are organized into two subcomplexes based on their association with AIMP2. Subcomplex I contains MRS, AIMP3, EPRS, IRS, LRS, KRS, and DRS and subcomplex II is composed of AIMP1, QRS, and RRS. aaRSs without GST-like domain are represented by pentagons, which are colored in *dark gray* when the enzyme is homodimeric. *C*, three types of interfaces can form between GST-like domains. Two canonical interaction modes are observed in GST-like dimers, which occur *via* interface 1 (through parallel helices α2 and α3) or interface 2 (through helices α7). *P. vivax* tRip dimerizes through an alternative interface 1 (44), where helices α2 and α3 of each monomer are oriented perpendicularly and contacts between α2–α2′ and α3–α3′ are observed. As a result, the β strands of the thioredoxin subdomain are oriented on the same side of the dimer. Interfaces 1 and 2 are indicated numerically throughout this figure. aaRS, aminoacyl-tRNA synthetase; AIMP, aaRS-interacting multifunctional protein; ARS, alanyl-tRNA synthetase; DRS, aspartyl-tRNA synthetase; ERS, glutamyl-tRNA synthetase; EPRS, glutamyl–prolyl-tRNA synthetase; IRS, isoleucyl-tRNA synthetase; KRS, lysyl-tRNA synthetase; LRS, leucyl-tRNA synthetase; MRS, methionyl-tRNA synthetase; MSC, multi-aaRS complex; PRS, prolyl-tRNA synthetase; RRS, arginyl-tRNA synthetase; QRS, glutaminyl-tRNA synthetase; tRip, tRNA import protein.

where YRS is the only protein without a GST-like domain (14). Among the six aaRSs (MRS, QRS, prolyl-tRNA synthetase (PRS), aspartyl-tRNA synthetase (DRS), tryptophanyl-tRNA synthetase (WRS), and alanyl-tRNA synthetase (ARS)) and the three AIMPs (MCP1, MCP2, and MCP3) that constitute the *T. brucei* MSC, MCP1, and MRS contain GST-like domains (15). In the vertebrate MSC, the largest and most intricate MSC, crucial interactions involve GST-like domains and other types of interaction motifs such as leucine-zippers and WHEP domains (9). Two AIMPs (AIMP2 and AIMP3 (p18)) and two aaRSs (MRS and bifunctional glutamyl–prolyl-tRNA synthetase (EPRS)) display GST-like domains. Together with AIMP1 and seven other aaRSs (QRS, DRS, lysyl-tRNA synthetase (KRS), arginyl-tRNA synthetase (RRS), isoleucyl-tRNA synthetase (IRS), and leucyl-tRNA synthetase (LRS)), they form a bisymmetrical complex (31–33).

Several crystal structures of MSC subcomplexes involving GST-like domains are available. The GST-like fold consists of two subdomains (34, 35) (Fig. 1*C*): the N-terminal thioredoxin-fold containing four β-strands (β1 to β4) and two helices (α1 and α2) and the C-terminal subdomain, which adopts an α-helical structure (α3 to α8). The central helix (α5) is mostly composed of hydrophobic residues and exhibits the N-capping box (S/T-X-X-D), which is strictly conserved and crucial for the stability of the fold (36, 37). GST-like modules interact using two conserved interfaces. The dimerization interface 1 involves mainly polar residues within helices α2 and α3 of each GST-like monomer in parallel orientation, similar to what was observed in catalytically active GST enzymes (34, 35). Dimerization through interface 2 involves the stacking of two arginines protruding from the α7 helix of each monomer and residues located in the loop connecting the α4 and α5 helices (38). Hence, Arc1p interacts with MRS through interface 1 (Protein Data Bank [PDB]: 2HSN) and with ERS through interface 2 (PDB: 2HRK) in the yeast MSC (38, 39). The same network of interactions allows the formation of the GST-like heterotetramer, which builds the core of the human MSC (40, 41), with AIMP3 and MRS (PDB: 4BVX) or AIMP2 and

EPRS (PDB: 5A34) dimerizing *via* interface 1 and AIMP3 and EPRS *via* interface 2 (PDB: 5BMU) (42).

In *Plasmodium*, the protozoan parasite responsible for malaria, a protein named tRNA import protein (tRip) has been identified (43); it is a fusion protein between a GST-like domain and an EMAPII-like domain, like *S. cerevisiae* Arc1p, *T. gondii* Tg-p43, and *T. brucei* MCP1 (Fig. 1*A*). However, tRip is an integral membrane protein localized to the parasite plasma membrane. It is implicated in an unprecedented tRNA trafficking pathway and, when the tRip gene is deleted, the development of the blood stage parasite is significantly reduced (43). Recently, the crystal structures of both domains (N-terminal GST-like and C-terminal EMAPII-like) of *Plasmodium vivax* tRip were solved independently (44). The N-terminal GST-like domain of tRip forms two types of dimers (PDB: 5ZKF). Two monomers interact either through the canonical interface 2 or through an alternative interface 1. In this unusual conformation, α2 and α3 helices of one monomer pack against α2 and α3 helices of the second monomer, but they are oriented perpendicularly to each other (and not parallel as it is the case in a canonical interface 1) (Fig. 1*C*). This situation is unique among structurally characterized GST-like dimers.

Thus, the combination between both its singular homodimeric conformation and its unusual role in tRNA import has raised questions about the implication of tRip in a *Plasmodium* MSC assembly. In this study, the existence of a tRip–bound MSC in the rodent malaria parasite *Plasmodium berghei* was experimentally verified. GST-like domains were used to determine their interaction patterns and infer the organization of the proteins in the parasite MSC. This approach led to an unexpected, novel observation: the interaction network between the different GST-like modules did not allow incorporation of all individual domains into a single MSC but rather led to the formation of two independent MSCs with specific biophysical properties *in vitro*.

Results

Identification of tRip partners in P. berghei *blood stages*

tRip and its partners were extracted from *P. berghei* blood-stage parasites using a purified and specific antibody raised against the C-terminal EMAPII-like domain of *Plasmodium falciparum* tRip (43). The strong lysis conditions resulting from saponin treatment significantly reduced the number of spectra in the b samples leading to its exclusion from the bioinformatics analysis. An average of 250 *P. berghei* proteins were thus identified in samples a, c, and d (three WT and three KO). As expected, tRip was found only in the WT samples. After subtraction of background interactions and protein frequency assessment, only four proteins were retained (ERS, MRS, QRS, and a nuclear ribosomal biogenesis regulatory protein) and considered statistically significantly increased in the WT sample, with an adjusted p value < 0.05, a minimum relevant spectral count of 5 (average), and a min Log fold change of 2 (Fig. 2*A* and Table S1). One candidate, ERS, stood out since its deltaSC and p value parameters were identical to those of tRip. Because of its nuclear localization and lack of detection in sample d, the ribosomal biogenesis regulatory protein was not considered further. Only one protein was significantly increased in the KO parasite (60S ribosomal protein L44, putative) compared to the WT.

Structural organization of selected aaRSs

The sequences of *P. berghei* tRip, ERS, QRS, and MRS were analyzed using Blast and multisequence alignments (MSAs)

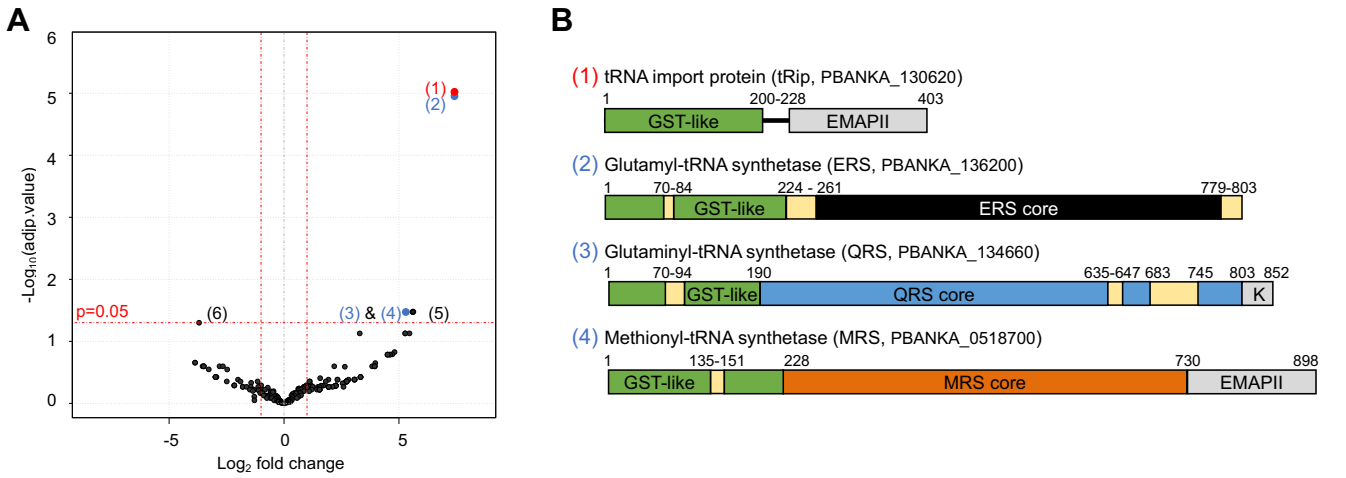

Figure 2. Identification of the tRip interactome in the *P. berghei* blood stage. *A*, volcano plot visualization of the tRip interactome. CoIP and mass spectrometry analysis (LC-MS/MS) of tRip partners were performed in three biological replicates, and LC-MS/MS data were analyzed by spectral counts. All identified proteins that were detected with more than five spectra were used for the generation of the differential expression test. Three aaRSs (2, 3, and 4) specifically bound to tRip (1) in all three samples with p values < 0.05, all of which have N-terminal GST-like domains. A nuclear protein involved in the ribosome biogenesis (5) was observed in two samples (a) and (c), and a ribosomal protein (6) was observed in the tRip-KO parasite in samples (a) and (d). Complete results are presented in Table S1. *B*, schematic representation of tRip and partners. aaRS cores are shown in *black* (ERS), *blue* (QRS), and *orange* (MRS), GST-like domains are shown in *green*, RNA-binding domains are shown in *gray*, and LCRs are shown in *pale yellow*; K indicates the K-rich C-terminal domain of *Plasmodium* QRS. aaRS, aminoacyl-tRNA synthetase; coIP, coimmunoprecipitation; ERS, glutamyl-tRNA synthetase; MRS, methionyl-tRNA synthetase; QRS, glutaminyl-tRNA synthetase; tRip, tRNA import protein.

(Fig. 2*B*). ERS, QRS, and MRS are all class I aaRSs characterized by HIGH and KMSKS motifs in their catalytic domains. Compared to their prokaryotic homologs, they contain additional sequences appended to their N- and C-terminal ends and several *Plasmodium*-specific insertions referred as low-complexity regions (LCRs). The length and composition of LCRs are generally variable between *Plasmodium* species and strains, but their localization is conserved within homologous proteins (45, 46). The longest LCRs are mainly observed in *P. falciparum* proteins and are characterized by long asparagine (N) repeats (47).

P. berghei tRip, ERS, QRS, and MRS sequences were then submitted to the Raptor X web server (http://raptorx.uchicago.edu/) (48) for 3D structure prediction. The Raptor X models were consistent with the Blast and the MSA analysis, and the top templates used to model each domain are shown in Table S2. All three aaRSs contained an N-terminal GST-like domain; MRS contained an EMAPII-like domain appended to its C terminus, while QRS had a C-terminal extension that was too short to be considered as an independent domain by Raptor X. Nevertheless, this extension contains many positively charged residues and has the potential to form one or more helices, suggesting RNA-binding properties (49–51) (Fig. S1, *A–F*). The prediction of C-terminal domains with potential tRNA-binding abilities in MRS and QRS led us to test whether these domains could bind tRNAs *in vitro*. Indeed, the presence of these C-terminal domains increased the interaction of the MRS and QRS anticodon-binding domains toward total human tRNA (Fig. S1, *G* and *H*), indicating that their binding were sequence nonspecific. These extensions are also conserved in MRS and QRS from other *Apicomplexan* parasites such as *T. gondii* (14).

GST-like domains mediate Plasmodium *MSC assembly*

Production of full-length ERS, QRS, and MRS led to low expression, limited solubility, or proteolysis of the recombinant enzymes, and mass spectrometry (MS) analyses revealed that recombinant ERS and QRS lacked their N-terminal GST-like domains. Moreover, none of these purified recombinant proteins interacted with tRip (Fig. S2). We therefore chose to focus specifically on the GST-like domains from each aaRS to investigate their interactions with each other and tRip. From here on, these domains are referred to as ERS-N ($ERS_{1\text{-}228}$), QRS-N ($QRS_{1\text{-}208}$), and MRS-N ($MRS_{1\text{-}228}$). Several constructs with and without a C-terminal 6His ($_{\text{-}6H}$) or SUMO-6His ($S_{\text{-}6H}$) tag were designed (Table S3). The SUMO domain not only slightly improved the solubility of MRS-N and QRS-N, but it also provided proteins of different sizes that could be distinguished one from each other on SDS-PAGE. Each partner was alternatively used as bait or prey in pull-down assays. In these assays, mixture of bacteria expressing (i) the 6His-tagged bait protein and (ii) one or more prey proteins was lysed and the protein extract was incubated with nickel-nitrilotriacetic acid (Ni-NTA) resin. This resin binds the bait protein and indirectly captures any prey protein through noncovalent interactions with the bait. After incubation, the resin was washed thoroughly, and the bound proteins were eluted and analyzed by SDS-PAGE. If an interaction occurred, bait and prey proteins appear together in the elution fraction.

Pairwise interactions showed that ERS-N associates with the other three domains (Figs. 3*A* and S3*A*); that MRS-N interacts with QRS-N and that MRS-N and ERS-N homo-oligomerize. As expected, the C-terminal domain of tRip was dispensable for its interaction with ERS-N, indicating that its GST-like domain is sufficient for complex assembly. However, the presence of the 6His tag directly attached at the ERS-N C terminus reduces its ability to interact with QRS-N. Similarly, a 6His tag directly linked to the C terminus of MRS-N abolishes any pairwise interaction. Thus, subsequent pull-down assays were performed with SUMO-tagged baits.

Pull-down assays with all four partners were performed, using alternative baits ($_{6H\text{-}}$tRip, ERS-N-$S_{\text{-}6H}$, QRS-N-$S_{\text{-}6H}$, and MRS-N-$S_{\text{-}6H}$). Individually, $_{6H\text{-}}$tRip and ERS-N-$S_{\text{-}6H}$ allowed the pull down of the other three proteins showing that each of these proteins interacts with all MSC components (Fig. S3*B*). In contrast, QRS-N-$S_{\text{-}6H}$ and MRS-N-$S_{\text{-}6H}$ led to the efficient capture of tRip and ERS-N but also to the apparent loss of the fourth partner (Fig. 3*B*). MS analysis corroborated the profile observed on the analytical gels. While MRS-N and QRS-N are present in comparable amounts with ERS-N-$S_{\text{-}6}$ as the bait, this equilibrium is disrupted when the bait is either MRS-N-$S_{\text{-}6H}$ or QRS-N-$S_{\text{-}6H}$ (bar charts in Fig. S3*B* and data in Table S1). Because it is difficult to control the amount of each recombinant protein in the samples, we performed competition experiments between QRS-N and MRS-N for binding to the tRip–ERS-N subcomplex. In these assays, tRip–ERS-N–MRS-N-$S_{\text{-}6H}$ and tRip–ERS-N–QRS-N-$S_{\text{-}6H}$ ternary complex were challenged with increasing concentrations of competitors, QRS-N or MRS-N, respectively (Fig. 3*C*). In both cases, we observe not only that the competitor does not integrate a quaternary complex but also that tRip–ERS-N gradually vanishes in the presence of the highest competitor concentrations (Fig. S3*C*), suggesting the formation of the alternative ternary complex lacking a 6His tag and thus eliminated during washes. Additional controls were performed with two other GST-like domains (Fig. 3*D*). On the one hand, the N-terminal GST-like domain of human EPRS fused to the $SUMO_{\text{-}6H}$ tag (*Hs*EPRS-N-$S_{\text{-}6H}$) was used in place of ERS-N-$S_{\text{-}6H}$ as a bait. On the other hand, the N-terminal GST-like domain of *P. berghei* EF1Bγ was tested as a prey for its ability to substitute for MRS-N, QRS-N, or tRip in pull-down experiments. None of these control domains could be incorporated into the complexes, indicating that the SUMO module does not promote the integration of nonspecific GST-like domains and that the interactions that drive complex formation are highly specific.

Finally, triplicates of large-scale pull-down experiments were performed using ERS-N-$S_{\text{-}6H}$, QRS-N-$S_{\text{-}6H}$, or MRS-N-$S_{\text{-}6H}$ as baits to further purify the different complexes by size-exclusion chromatography (SEC) and analyze them by MS (Fig. 4). In all cases, the captured proteins eluted as a main peak with comparable elution volumes on SEC, indicating the formation of soluble complexes with apparent molecular weights (MWs) of 300 to 400 kDa (Fig. 4*A*). Pull down with

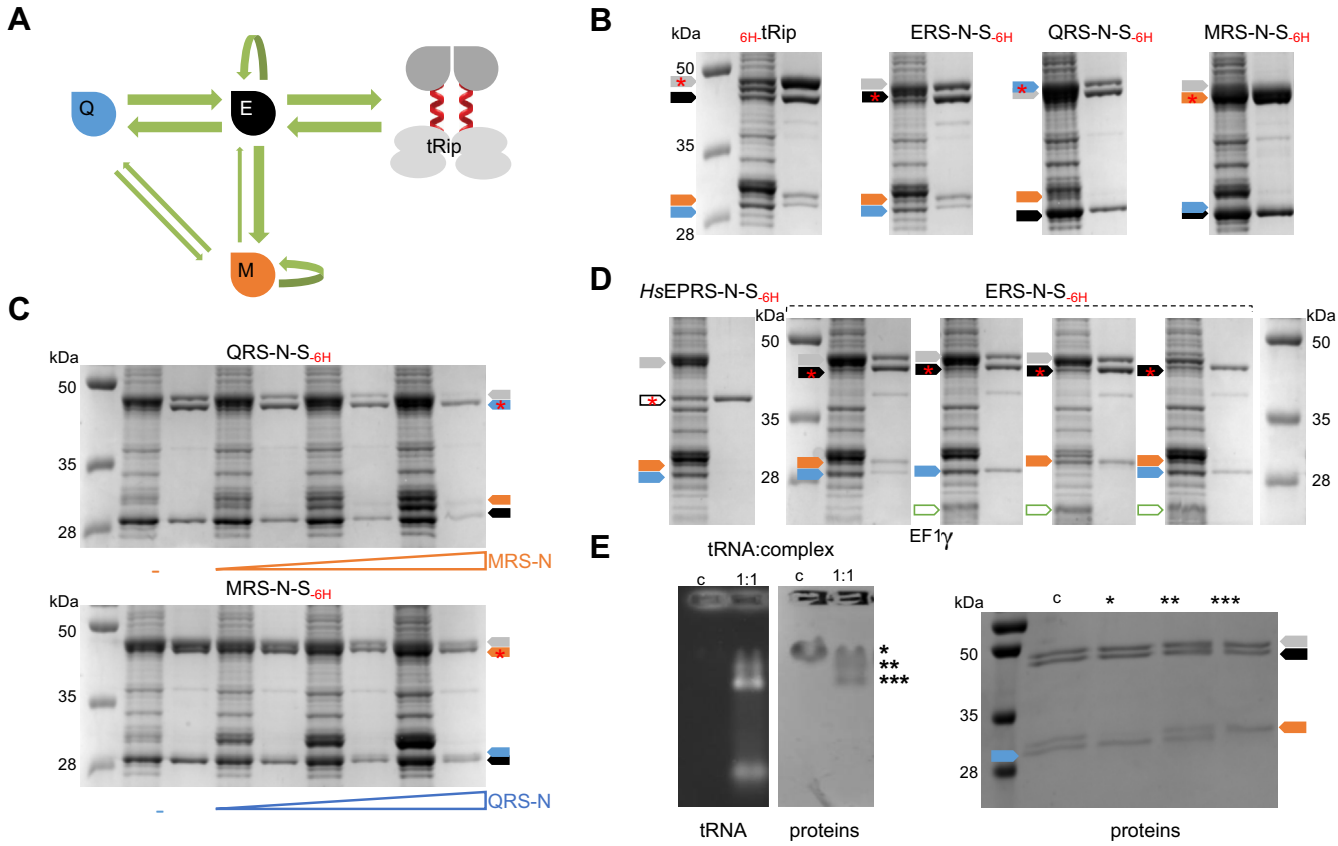

Figure 3. Interaction between *P. berghei* tRip, ERS, MRS, and QRS GST-like domains. *A*, summary of pairwise interactions. Results of pull-down experiments performed with two GST-like domains (Fig. S3*A*) are shown (n ≥ 3). The *thick arrows* indicate the most effective interactions and the *thin arrows* the weakest interactions. *B*, pull-down experiments with four proteins. Each protein was used as bait to test for capture of the other three (n ≥ 3). The content of the initial mixture and the captured proteins are shown on each gel. Partners are identified in *gray* (tRip), *black* (ERS-N-S or ERS-N), *blue* (QRS-N-S or QRS-N), and *orange* (MRS-N-S or MRS-N) *arrows*; the bait protein is indicated by a *red asterisk*. MRS-N-S and tRip as well as ERS-N and QRS-N comigrate. The additional bands present on the gels could correspond to either *E. coli* EF-Tu or outer membrane proteins A; these proteins are about 40 kDa and are among the most abundant contaminants (Table S1). *C*, competitions; series of pull-down experiments were performed with constant concentrations of QRS-N-S$_{-6H}$–tRip–ERS-N or MRS-N-S$_{-6H}$–tRip:ERS-N and increasing concentrations of MRS-N or QRS-N, respectively. *D*, specificity controls; the GST-like domain present at the N terminus of human glutamyl-prolyl-tRNA synthetase (EPRS) was fused to the SUMO$_{-6H}$ tag (*Hs*EPRS-N-S$_{-6H}$) (*empty black arrow*) and replaced the ERS-N-S$_{-6H}$ bait in the pull-down experiment with four partners. Alternatively, the N-terminal GST-like domain of *P. berghei* EF1Bγ (*empty green arrow*) was used as prey in place of MRS-N, QRS-N, and tRip. *E*, segregation of complexes upon tRNA binding. The four proteins were copurified using ERS-N-S as bait and tested for their capacity to bind yeast total tRNA. With a tRNA:complex ratio of 1:1, assuming the complex is monomeric, three bands (*, **, and ***) were observed in a 1% agarose gel after RNA and protein visualization with ethidium bromide and Coomassie blue staining, respectively. The bands were cut out and their protein content was analyzed by SDS-PAGE (n = 3). ERS, glutamyl-tRNA synthetase; MRS, methionyl-tRNA synthetase; QRS, glutaminyl-tRNA synthetase; tRip, tRNA import protein.

either QRS-N-S$_{-6H}$ or MRS-N-S$_{-6H}$ led to the purification of heterotrimeric complexes that excluded MRS-N or QRS-N, respectively (Fig. 4, *B* and *C*). Although a heterotetrameric complex cannot be ruled out, these observations are consistent and strongly suggest the existence of two mutually exclusive heterotrimeric complexes *in vitro*: tRip–ERS-N–QRS-N and tRip–ERS-N–MRS-N. For convenience, these heterotrimers are referred as Q-complex and M-complex, respectively.

Oligomeric state of Q- and M-complexes in solution

Q- and M-complexes were purified with QRS-N-S$_{-6H}$ and MRS-N-S$_{-6H}$ baits, respectively. SUMO fusions were proteolytically removed before the final purification step on a calibrated SEC column (Fig. 5*A*). As expected, the main peaks contained heterotrimeric complexes consisting of equivalent amounts of each partner, as assessed by SDS-PAGE (Fig. 5*B*) and further confirmed that the SUMO-tag is not involved in the complex association. The apparent MWs of the Q- and M-complexes derived from the SEC profiles (about 250 and 275 kDa, respectively), indicated that both complexes (with theoretical MWs of 97 kDa and 101.5 kDa, respectively) were elongated or oligomerized. Thus, their size and homogeneity were further investigated by batch light-scattering measurements. On the one hand, dynamic light scattering (DLS) indicated homogeneous samples (Fig. 5*C*) and measured MW-R (MW based on hydrodynamic radius) of 295 and 393 kDa assuming spherical particles for the Q- and M-complexes, respectively. On the other hand, static light scattering (SLS) yielded MW-S (absolute MW) of 204 and 247 kDa for the two complexes, respectively. These measurements indicate not only that the complexes contained at least two copies of each partner but also that they had an elongated conformation (MW-R/MW-S > 1). Only SEC–multiangle light scattering (MALS) could establish more precisely the oligomeric state of the complexes (Fig. 5*D*).

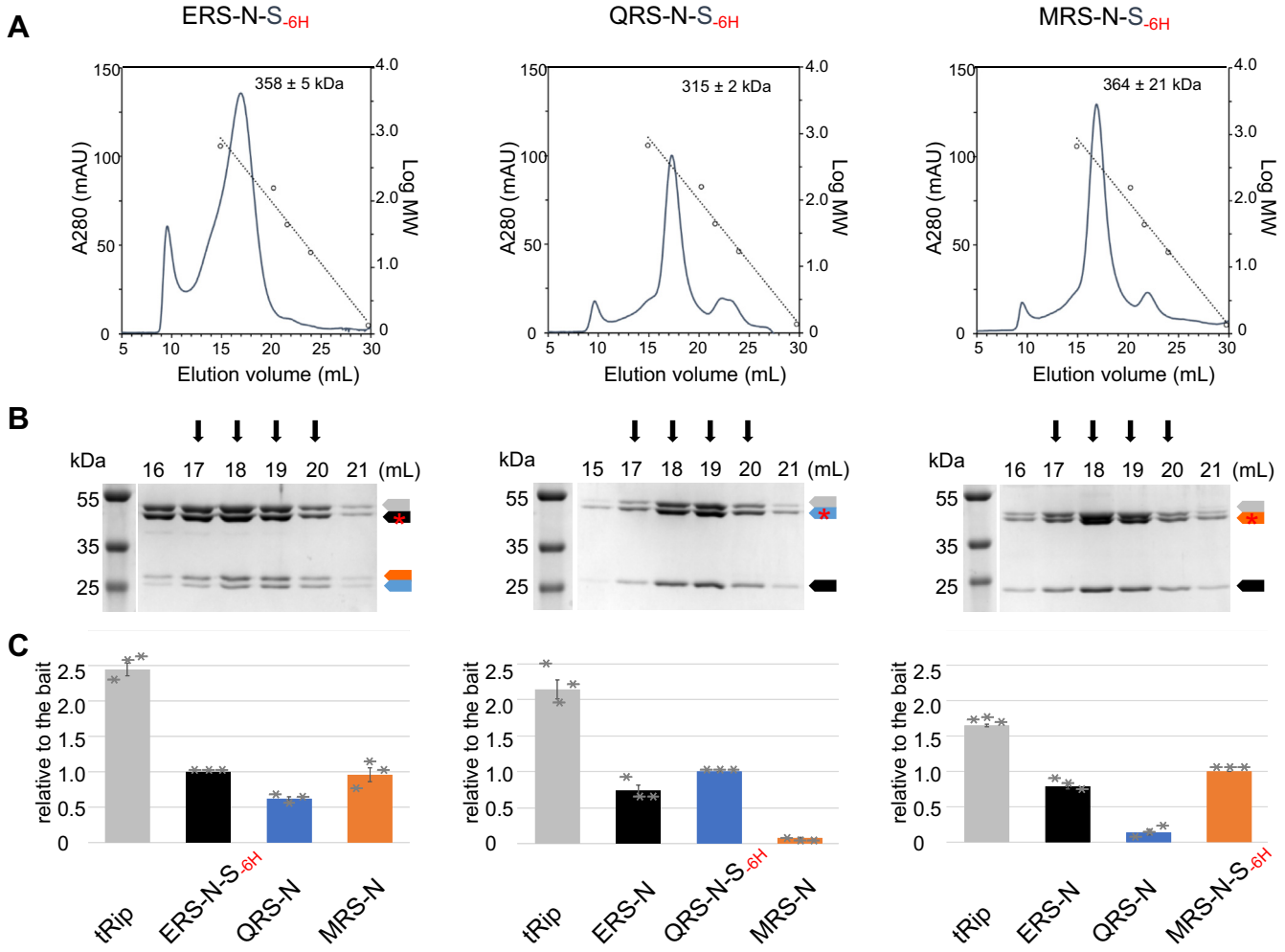

Figure 4. Composition of complexes. Bacteria expressing the tRip and other GST-like partners were lysed together and protein extracts were subjected to Ni-affinity and size-exclusion chromatographies (SECs). Different baits (ERS-N-S$_{-6H}$, QRS-N-S$_{-6H}$, or MRS-N-S$_{-6H}$) were used to capture the different preys (tRip, ERS-N, QRS-N, and MRS-N). *A*, SEC chromatograms. Complexes eluted as a main peak on a SepFast 6 to 5000 kDa (n > 3) column. Graphs show the elution profile (*left axis*) and calibration curve (*right axis*, $R^2 = 0.98$) based on the elution of the following size markers: thyroglobulin (669 kDa), γ-globulin (158 kDa), ovalbumin (44 kDa), myoglobin (17 kDa), and vitamin B12 (1.35 kDa). *B*, SDS-PAGE analysis. Fractions of the main SEC peak were analyzed by SDS-PAGE. *C*, mass spectrometry. Fractions marked with arrows (in *panel B*) were pooled and analyzed by mass spectrometry. Three independent experiments were performed, and the relative abundance of each partner (based on the number of spectra) was plotted. Colors were maintained: *gray* for tRip, *black* for ERS-N, *blue* for QRS-N, and *orange* for MRS-N. Error bars represent SD across the triplicate measurements. Purification of complexes on SEC led to more homogeneous samples for mass spectrometry analysis. ERS, glutamyl-tRNA synthetase; MRS, methionyl-tRNA synthetase; QRS, glutaminyl-tRNA synthetase; tRip, tRNA import protein.

While the Q-complex yielded a MW of 187.3 kDa, close to the expected value for a dimeric heterotrimer (193.6 kDa), the M-complex showed overlapping oligomeric species. The major peak indicated a value of about 217 kDa, corresponding to the theoretical MW of a dimeric heterotrimeric M-complex (203 kDa), yet an additional population was not completely separated by the column and was characterized by a larger size around 500 kDa. This size estimation corresponds to two to three copies of the dimeric ternary complex, suggesting that the M-complex might oligomerize further in solution. This observation was supported by light-scattering experiments on MRS-N, which showed that at a concentration suitable for measurements (*i.e.*, 1.8 mg/ml), most MRS-N-S$_{-6H}$ molecules appear as elongated dimers; yet, populations with higher apparent sizes were visualized by SEC and DLS/SLS analysis (Fig. S4*A*).

Two types of ternary GST-like complexes with different tRNA-binding profiles

EMSAs with individual Q- and M-complexes (purified with QRS-N-S$_{-6H}$ or MRS-N-S$_{-6H}$) in the presence of yeast total tRNA revealed specific migration profiles (Fig. S5). Control experiments using complexes lacking the EMAPII-like domain (tRip-N) confirmed that tRNA binding was specific to the C-terminal domain of tRip. Furthermore, all three proteins were present in the tRNA-bound fraction (Fig. S5), indicating that the complexes did not dissociate upon tRNA binding.

Alternatively, in EMSA performed with the complexes purified with ERS-N-S$_{-6H}$ bait in the presence of tRip, QRS-N and MRS-N also shifted the tRNAs but showed three populations (Fig. 3*E*). The corresponding bands were cut out and analyzed by SDS-PAGE to determine their protein content. The upper band (*) contained only the Q-complex while the bottom band

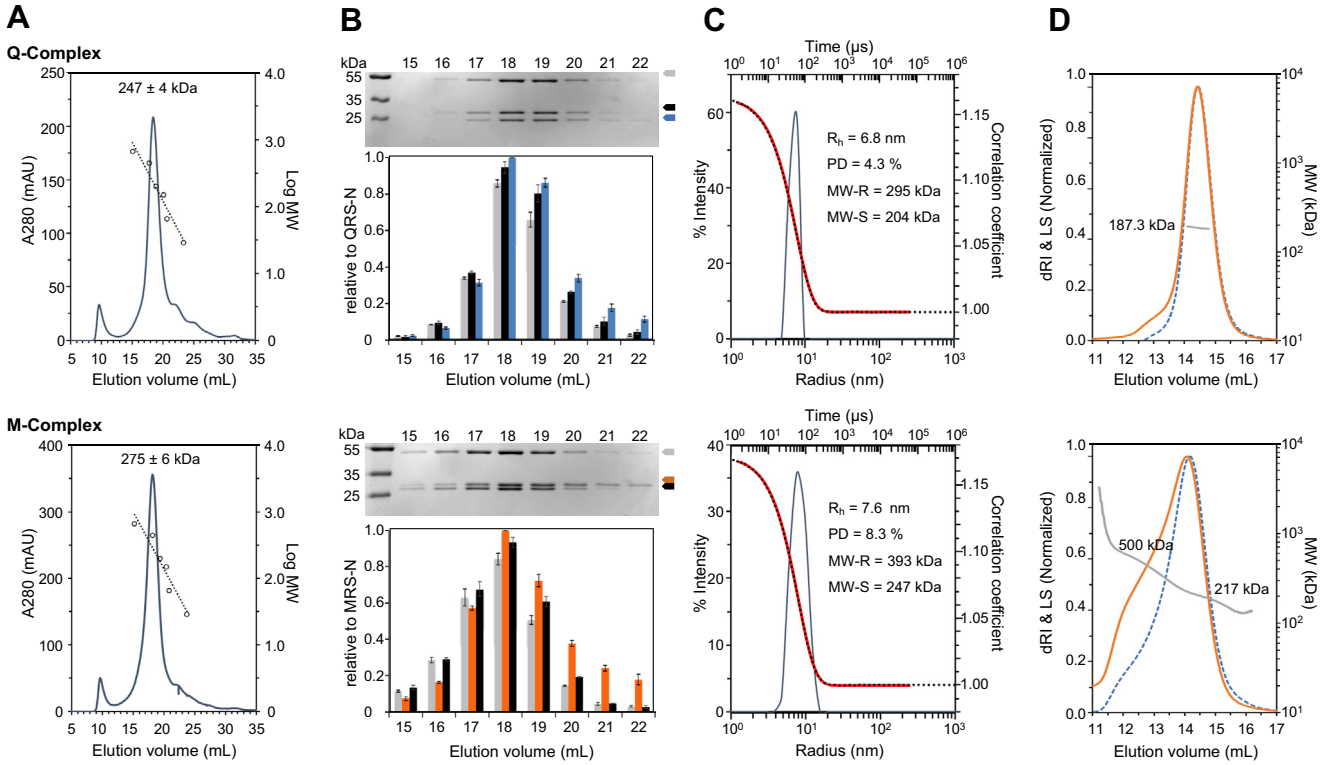

Figure 5. Purification and characterization of *Plasmodium* Q- and M-complexes. Q- and M-ternary complexes were purified using QRS-N-S$_{-6H}$ and MRS-N-S$_{-6H}$ as respective baits in the presence of tRip and ERS-N. *A*, SEC experiments. The SUMO tags were removed by TEV cleavage, and the complexes were applied to a calibrated SepFast 6 to 5000 kDa column (n > 3). Graphs show the elution profile (*left axis*) and calibration curve (*right axis*, R^2 >0.9) based on the elution of the following size markers: thyroglobulin (669 kDa), apoferritin (443 kDa), β-amylase (200 kDa), alcohol dehydrogenase (150 kDa), bovine serum albumin (66 kDa), and carbonic anhydrase (29 kDa). *B*, fraction analysis by SDS-PAGE and quantification. The relative amount of each partner was quantified in the SEC peaks from (*A*). Fractions containing equimolar amounts of domains were pooled and used in light-scattering measurements. *C*, DLS/SLS experiments. Graphs show the intensity-based particle size distribution (*left y*-axis) as a function of particle radius (*lower x*-axis), and the experimental data (*black dots*) as well as the cumulant-fitted autocorrelation function (*red line*) (*right y*-axis) as a function of time (*upper x*-axis). The Q- and M-complexes were assayed at concentrations of 3.7 and 4.1 mg/ml, respectively. Hydrodynamic radius (Rh), polydispersity (PD), molecular weight (MW-R) derived from Cumulants DLS analysis, and the absolute molecular weight (MW-S) inferred by SLS are indicated. *D*, SEC-MALS experiments. Elution profiles of Q- and M-complexes on a Superose 6 column are shown. Normalized light scattering (LS, *orange*) and differential refractive index (dRI, *blue*) are on the *left y*-axis and molecular weights (*gray*) on the *right y*-axis. While the Q complex is homogeneous and appears as a dimer, SEC separation did not provide dimer–oligomer resolution for the M-complex (n = 2). DLS, dynamic light scattering; ERS, glutamyl-tRNA synthetase; MALS, multiangle light scattering; MRS, methionyl-tRNA synthetase; QRS, glutaminyl-tRNA synthetase; SLS, static light scattering; tRip, tRNA import protein.

(***) contained only the M-complex. This segregation upon tRNA binding supported our hypothesis that the proteins copurified with ERS-N-S$_{-6H}$ form two independent heterotrimeric complexes. Yet, all four proteins were observed in the middle band (**), probably because of an overlap of the two ternary complexes.

Mapping interaction interfaces in Q- and M-complexes

In the presence of two exclusive heterotrimeric complexes organized around the tRip–ERS-N heterodimer and containing either QRS-N or MRS-N, we chose to test the effect of point mutations in pull-down experiments with ERS-N-S$_{-6H}$ as the bait and all three preys (tRip, QRS-N, and MRS-N) together. This approach allowed us to assess whether the mutations had a global impact on both complexes or had a specific effect on the formation of a given one (Q or M). The list of mutations and their effect on pull-down assays are summarized in Figure 6*A* (list of mutations), Figure 6*B* (results summary), and Figs. S6 (sequence alignments) and S7 (experimental data).

tRip is a homodimer in solution, as shown by light-scattering analysis (MW-S = 114 kDa, only slightly larger than the calculated 92.4 kDa). In addition, the shape factor deduced from these measures (MW-R/MW-S > 1) suggests that tRip is an elongated dimer (Fig. S4*B*), which associates *via* a unique interaction as seen in the crystal structure of tRip-N (44) (Fig. 1*C*). This alternative interface 1 mainly involves phenylalanine residues: F58 in helix α2 and F90 in helix α3 (Fig. S6*A*). Independent mutation F58A and F90A did not impair tRip–ERS-N heterodimerization or the formation of the Q-complex but specifically hindered the association of MRS-N into the M-complex.

Among the four GST-like partners, only tRip and ERS-N contain a strictly conserved arginine in their respective α7 helices (Fig. S6*B*), suggesting that they might interact *via* a canonical interface 2 (Fig. S6*A*). As expected, tRip R154A and ERS-N-S$_{-6H}$ R198A completely abolished interactions between the two partners. Yet, the R198A mutation in ERS-N-S$_{-6H}$ also specifically inhibited the binding of MRS-N in the complex, indicating that ERS-N needs to bind tRip to bring MRS-N into the M-complex. In contrast, the dissociation between tRip and

A

Interface	localization	mutation	solubility	tRip	ERS-N	QRS-N	MRS-N
tRip							
Interface 1	α2	**F58A**	±	D	✓	✓	x
	α3	**F90A**	+	D	✓	✓	x
Interface 2	α7	**R154A**	+		x	x	x
ERS							
Interface 1	α2	S85A-S86A	+	✓		✓	✓
		D87A	-				
		I89R	+	✓		•	✓
		F90A	+	✓		✓	x
		A91R	-				
		N93A	+	✓		✓	✓
		L94R	-				
		D95A	-				
		L97R	+	✓		✓	•
		K99A	+	✓		✓	✓
	α3	**V120R**	+	✓		✓	•
		F121A	+	✓		✓	✓
		Q123A	+	✓		✓	✓
		A124R	+	✓		•	•
		Y126A	+	✓		✓	✓
		N127A	+	✓		✓	✓
		E128A	+	✓		x	✓
		D131A	+	✓		x	✓
		F132A	+	✓		✓	✓
Interface 2	α7	**R134A**	+	✓		✓	✓
		R198A	+	x		✓	x
QRS-N							
Interface 1	α2	**N62A**	+		x		
		E65A	±		✓		
		V66R	+		•		
		H69A	+		✓		
	α3	K97A	+		✓		
		V99R	+		•		
		E102A	+		✓		
		E103A	+		✓		
		K105A	+		x		
		K109A	+		x		
MRS-N							
Interface 1	α2	**S61A-S62A**	-				
		A65R	+		•		
		F68A	+		x		
		L69R	±		✓		
		H71A	±		x		
	α3	**L87R**	-				
		Y90A	+		x		
		W93A	-				
		E95A	+		x		
		S97A	±		✓		
		D98A	±		✓		
		E101A	±		✓		
		K102A	±		✓		
Interface 2	α7	**Δα7**	-				

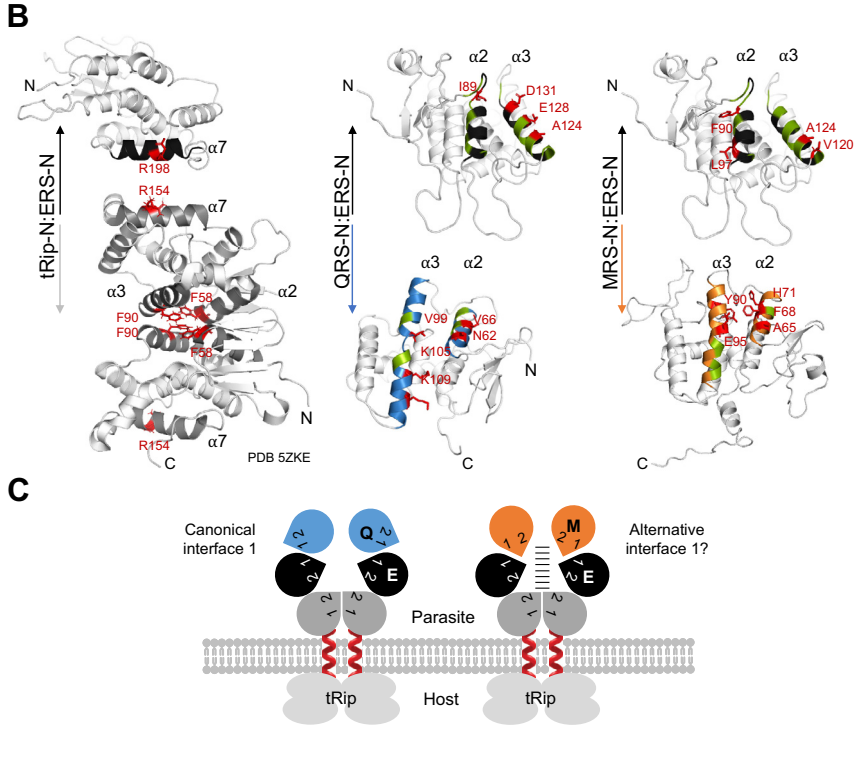

Figure 6. Arrangement of GST-like domains in Q- and M-ternary complexes. *A*, probing of GST–GST interactions between tRip, ERS-N, QRS-N, and MRS-N. Bold residues correspond to conserved residues present in helices 2, 3, and 7 of the N-terminal GST-like domains of tRip, ERS, MRS, and QRS. The effects of the mutations are indicated with different symbols: (✓) no effect on heterodimerization; (•) the replacement of a small uncharged amino acid (alanine, leucine, or valine) with a large charged amino acid (arginine) interfered with the proximity between GST domains; (x) alanine replacements disrupted the interaction between GST domains. *Gray boxes* indicate that amino acid mutation led to the complete destabilization of the mutated protein and (D) indicates amino acids that are involved in homodimerization. Each interaction was tested by pull-down assays at least three times. *B*, modeling of the GST-like interfaces. All amino acids tested are shown on the crystal structure of *P. vivax* tRip (PDB: 5ZKE) and Raptor X models of ERS-N, QRS-N, and MRS-N. Models are shown in *light gray* and the domains investigated by mutagenesis are shown in *dark gray* (tRip), *black* (ERS-N), *blue* (QRS-N), or *orange* (MRS-N). Silent mutations are shown in *green* and the mutations leading to the disruption of the complexes are labeled and shown with *red sticks C*, schematic representation of the two ternary complexes identified in *P. berghei*. Models based on this study show two complexes containing two copies each of membrane-bound tRip, ERS-N, and either QRS-N (Q-complex) or MRS-N (M-complex). The interaction interfaces of each partner according to mutagenesis experiments are indicated. Inclusion of MRS-N in the M-complex depended on both tRip dimerization and tRip–ERS-N interaction (*dashes*). ERS, glutamyl-tRNA synthetase; MRS, methionyl-tRNA synthetase; PDB, Protein Data Bank; QRS, glutaminyl-tRNA synthetase; tRip, tRNA import protein.

ERS-N did not affect binding between QRS-N and ERS-N-$S_{\text{-6H}}$ in the Q-complex.

To initiate the investigation of interfaces connecting ERS-N and QRS-N or MRS-N, we used the same approach as (38, 41, 42). Small uncharged amino acids (alanine (A), valine (V), isoleucine (I), or leucine (L)), when present on the surface of helices α2 and α3, were replaced with the large and charged arginine (R) to disrupt any proximity contacts between potentially interacting surfaces. In ERS-N, only A124R (α3) interfered with both Q- and M-complexes, whereas I89R (α2) specifically disrupted the Q-complex, and L97R (α2) and V120R (α3) specifically disrupted the M-complex, suggesting that QRS-N and MRS-N recognized ERS-N interface 1 but do not share interaction patterns. Since the GST-like canonical interface 1 is globally polar, as shown by the crystal structure of the human MRS–AIMP3 and EPRS–AIMP2 heterodimers and, to a lesser degree, that of the yeast MRS–Arc1p heterodimer (Fig. S6*A*), we looked for conserved polar residues in helices α2 and α3 in ERS-N. Mutations of D87A or D95A in α2 destabilized ERS-N, while R134A (α3) did not have any effect on Q- or M-complex formation. E128A and D131A mutations in α3 disrupted only the Q-complex.

In the mirror experiment R replacements of V66 (α2) or V99 (α3) as well as mutations of N62A (α2), K105A (α3), and K109A (α3) in QRS-N, disrupted QRS-N uptake into the Q-complex (Fig. 6*A*). The participation of so many polar residues in the ERS-N–QRS-N interaction is reminiscent of what has been shown in human heterodimers, especially between EPRS and AIMP2 (42).

Association between ERS-N and MRS-N was less obvious. Indeed, only an A65R mutation in MRS-N α2 disrupted its interaction with the M-complex, and the mutation of most of the polar amino acids present in α3 (D98A, E101A, and K102A) had no effect, except for E95A. Helices α2 and α3 contain several aromatic residues (Fig. S6*B*), as it is the case in tRip α2 and α3 (44). Only mutations of F68A (α2), H71A (α2), or Y90A (α3) in MRS-N and of F90A (α2) in ERS-N-$S_{\text{-6H}}$ led to the specific disruption of the M-complex, suggesting that MRS-N might interact with ERS-N *via* an alternative interface 1 (Figs. 6 and S6*A*).

Discussion

In this study, we immunoprecipitated, under stringent selection conditions, proteins interacting with the endogenous

P. berghei tRip. The identified interactome only contained aaRSs. These aaRSs catalyzed the specific aminoacylation of tRNAs with glutamate (ERS), methionine (MRS), and glutamine (QRS) (Fig. 2*A*). As in tRip, all three *Plasmodium* aaRSs contain GST-like domains at their N termini (Fig. 2*B*). Only six *Plasmodium* proteins containing a GST-like domain were identified in the conserved domain database (CDD) (52). They corresponded to tRip, ERS, MRS, the elongation factor 1β (EF1β, PBANKA_081420), the GST-1 (PBANKA_10239), and the thioredoxin-GST-EF1Bγ (PBANKA_135200). The N-terminal GST-like domain of QRS was not considered as such in the CDD, probably due to the low sequence conservation and the presence of an LCR in the middle of the structural fold. However, further investigations, including its modeling with Raptor X, allowed its detection (Fig. 2 and Table S2).

Based on aaRSs composition, the closest MSCs to the *Plasmodium* MSC were those from *S. cerevisiae* (53) or *T. gondii* (14), both of which have been characterized as cytosolic. The purification of *T. gondii* MSC led to significantly heterogeneous samples in size and composition (14). In contrast, the *S. cerevisiae* MSC is well defined and interactions between the three GST-like domains have been identified by crystallography (30, 38). The present study indicates that *P. berghei* harbors two MSCs, the Q- and M-complexe, each containing two copies of tRip, ERS-N and QRS-N or of tRip, ERS-N, and MRS-N, respectively. ERS-N has a central position, since it binds simultaneously to tRip, QRS-N, or MRS-N. Nevertheless, QRS-N and MRS-N diverge in their interaction pattern with ERS-N. While the association of MRS-N in the M-complex requires the presence of a dimeric tRip associated to ERS-N, QRS binds directly to ERS-N even in the absence of tRip (Fig. 6*A*). Moreover, mutational experiments confirmed that QRS-N and MRS-N bind to the same interface on ERS-N, but with two different strategies (Fig. 6*A*). Our favorite hypothesis is that interactions between QRS-N and ERS-N would mainly involve polar residues as in a GST–GST canonical interface 1 and that binding of MRS-N to ERS-N–tRip would use a different pattern closer to an alternative interface 1, with an aromatic environment (Fig. 6).

In yeast, the isolated EMAPII-like domain of Arc1p binds with high affinity and specificity to $tRNA^{Met}$ and $tRNA^{Glu}$ and strongly increases the affinity of MSC-associated MRS and ERS for their cognate tRNAs (19, 54). In contrast, the EMAPII-like domain of tRip is located on the parasite surface and thus theoretically cannot participate in tRNA aminoacylation within the parasite. The absence of this domain in the vicinity of the aaRSs could be balanced by the presence of the C-terminal extensions of *Plasmodium* QRS and MRS (Figs. 2 and S1). Indeed, these extensions had nonspecific RNA-binding capacities, although characterized by low affinities (Fig. S1*H*). The tRNA-binding capacity is generally low for such isolated domains, whether it is the human AIMP1 domain (55), the *Oryza sativa* C-terminal MRS domain (56), or the WHEP domain of the human EPRS (57). Yet, when fused to the core of aaRSs, these domains significantly increase the affinity of the enzymes for their cognate tRNAs. By analogy, the C-terminal domains of *Plasmodium* MRS and QRS could act synergistically and confer the ability to bind their cognate tRNAs with higher affinities to these enzymes to compensate for the membrane localization of tRip.

The EMAPII-like domain of *P. falciparum* tRip exhibits a unique specificity pattern. It discriminates tRNAs based on their posttranscriptional modification profiles, and tRip's preferred binders are isoacceptors of human host $tRNA^{Ala}$, $tRNA^{Ser}$, $tRNA^{Leu}$, and $tRNA^{Asn}$ (58), suggesting that import of exogenous tRNAs is not related to aminoacylation by MSCs' aaRSs. It is worth noticing that the single human $tRNA^{Asn}$ isoacceptor is not only one of the best ligands for tRip but also that asparagine is the predominant amino acid in the *P. falciparum* proteome. Most asparagine residues are found in LCRs and form long homopolymeric regions (46) suggesting that tRNA import may facilitate their synthesis. Although asparagine-rich insertions are present in virtually all *Plasmodium* proteins, their role is not yet established; these repeats are suspected to be involved in protein–protein interactions and/or aggregation, protein localization, immune response, or parasite virulence (59).

The two *Plasmodium* MSCs could differ in their ability to organize in the parasite membrane and might thus behave differently in tRNA aminoacylation, tRNA import, or any other alternative function of the associated aaRSs. Indeed, biophysical experiments showed that the M-complex is characterized by larger apparent sizes than those determined for the Q-complex (Fig. 5). Interestingly, pairwise pull-down assays and DLS/SLS experiments indicated that MRS-N had the ability to oligomerize (Figs. S3*A* and S4*A*), suggesting that it induces the oligomerization of the M-complex and thus its potential to open a portal in the parasite plasma membrane. Alternatively, binding of exogenous tRNAs to the outer EMAPII-like domain of tRip could be a signal to dissociate and relocalize complex-bound aaRSs to parasite organelles and thus trigger their involvement in alternative functions. Our *in vitro* experiments do not support the dissociation of the complex upon tRNA binding (Fig. S5), but the outcome may be different *in vivo.* Also, unlike yeast or human MRSs, which exhibit nuclear localization (23, 60), *P. falciparum* MRS was not observed in the nucleus at any of the blood stages, even in the presence of growth factors (61). Interestingly, these microscopy data also show that MRS is not homogeneously diffused in the schizonts' cytosol, a situation consistent with a membrane-bound enzyme. Similarly, the indirect aminoacylation pathway of the apicoplast $tRNA^{Gln}$ has been demonstrated (62), suggesting that the nuclear-encoded QRS has no aminoacylation function in this organelle.

tRip is an integral membrane protein that has been localized exclusively at the parasite surface at both the sporozoite stage (the infectious stage injected by mosquitoes into the vertebrate hosts) and the blood stage (43). To date, no other AIMP has been described with such localization, and, with the publication of the structure of the *P. vivax* tRip N-terminal domain, it appears that the transmembrane helix (α5) as we predicted (43) is deeply buried in the GST-like structure (44). Neither the crystal structure, nor the present study, have allowed identification of the transmembrane domain that anchors tRip

in the parasite plasma membrane; however, the unique symmetry identified in the crystal structure of the *P. vivax* tRip-N dimer positions the C-terminal extremities of each monomer in the same direction, which is critical to orient both EMAPII-like domains toward the outside of the cell, while the rest of the complex is located inside the cell to allow the formation of the two MSCs. Interestingly, there are scattered elements in the literature that suggest the possibility for GST-like domains to traverse/interact/bind cellular membranes. Amongst them, chloride intracellular channels are a unique class of ion channels, which exist as both soluble and membrane bound oligomers (63, 64). The ion channel hypothesis remains speculative. However, it has been demonstrated that chloride intracellular channels proteins have roles in diverse biological processes associated with membrane trafficking. They are often found associated with the actin cytoskeleton and to intracellular membranes (65, 66).

tRip is not the only RNA-binding protein found on the surface of *Plasmodium* sporozoites: polyA-binding protein-1 (PABP-1) of *Plasmodium yoelii*, homologous to cytosolic PABPs, is localized on the surface of sporozoites (67). Similarly, several studies have discovered that the glycolytic GAPDH is surface localized at several stages of the *P. falciparum* life cycle; especially, it plays an important role in liver infection by sporozoites (68, 69). Interestingly, among a variety of cellular processes, GAPDH has been implicated in the nuclear export of tRNAs, the stability and translation of mRNAs, and the replication and expression of several single-stranded RNA viruses (reviewed in (70)). Understanding why the parasite, particularly at the sporozoite stage, uses RNA-binding proteins on its surface may provide additional clues as to how it interacts with the host and/or other parasites.

Experimental procedures

Identification of tRip partners

Sample preparation

Four samples (biological replicates) of WT (GFPCON) blood stage of *P. berghei* parasites were assayed. Four negative control experiments were performed with the tRip-KO parasite (43) to define the background. Parasites were isolated from the blood of infected mice presenting parasitemia between 5 and 10%. The blood was centrifuged at room temperature for 10 min at 450 g to remove leukocytes. Pelleted erythrocytes were specifically lysed with different protocols: (a) by addition of erythrocyte lysis buffer (150 mM NH_4Cl, 100 mM $KHCO_3$, 10 mM EDTA, and 0.5% bovine serum albumin (w/v)) for 5 min on ice, (b) with saponin 0.1% (w/v) for 5 min on ice, and (c and d) by addition of activated streptolysin O (6000 U, 100 mM DTT) for 15 min at 37 °C. Samples were centrifuged for 8 min at 2000*g* and the supernatants were discarded. Pellets were resuspended in 1 ml PBS, and free parasites were separated from cellular debris by centrifugations (2 min at 100*g*) and transfer of the clean supernatant to a fresh tube. This operation was repeated four times until all contaminating cellular debris (especially intact red blood cells) were removed. Parasites were harvested by centrifugation for 8 min at 2000*g* and lysed in 1 ml cold extraction buffer (50 mM Tris–HCl pH 8.0, 150 mM NaCl, 1% Triton X-100, 10 mM DTT, and 1/50 protease inhibitor [cOmplete Tablets EDTA-free, Roche]) for 1 h on ice. Samples were mixed every 10 min, and the final cell lysate was centrifuged for 15 min at 10,000*g* to remove any insoluble material.

Coimmunoprecipitation

The coimmunoprecipitation (coIP) protocol was established by combining the kit protocol (MultiMACS Protein A/G MicroBeads kit; Miltenyi Biotec) with protocols described in (71, 72). Briefly, parasite extracts (500 µg) were incubated with protein A-coated magnetic beads (50 µl/ml) for 30 min at 4 °C under gentle agitation. The cleared sample (1 ml) was then incubated with 6 µg of purified anti-$tRip_{214\text{-}402}$ antibody and 50 µl of beads for 1 h under gentle agitation at 4 °C and loaded on a microcolumn applying a magnetic field. Successive washes (200 µl) were performed: twice with salt-free buffer (50 mM Tris–HCl pH 8.0, 1% NP-40), once with intermediate salt buffer (50 mM Tris–HCl pH 8.0, 150 mM NaCl, 1% NP-40), once with high salt buffer (50 mM Tris–HCl pH 8.0, 500 mM NaCl, 1% NP-40), and twice with salt-free buffer. Proteins bound to anti-$tRip_{214\text{-}402}$ antibodies were eluted in 150 µl denaturing buffer (50 mM Tris–HCl pH 6.8, 50 mM DTT, 1% SDS, 0.025% bromophenol blue, and 10% glycerol) at 95 °C.

MS and data analyses

Eluted proteins were precipitated, reduced, and alkylated as described in (73). Proteins were digested overnight with sequence-grade porcine trypsin (1:25, w/w; Promega), and generated peptides were analyzed on a NanoLC-2DPlus system (nanoFlexChiP module, Eksigent, AB Sciex) coupled to a TripleTOF 5600 mass spectrometer (AB Sciex) operating in positive mode. Peptides were loaded on a trap-and-eluate setup of C18 reverse-phase columns (ChiP C-18 precolumn 300 µm ID × 5 mm ChromXP and ChiP C-18 analytical column 75 µm ID × 15 cm ChromXP, Eksigent) in solvent A (0.1% formic acid in water) and separated with a 120 min gradient (5% to 40%) of solvent B (0.1% formic acid in acetonitrile) at a 300 nl/min flow rate. The mass spectrometer was operated in high-sensitivity data-dependent acquisition mode with Analyst software (v1.6, ABS ciex) on a 400 to 1250 m/z range. An external calibration was performed before each sample by monitoring 10 peptides of a β-galactosidase tryptic digest. A discovery "Top 20" method was used to select the most intense multiple-charged ions (2+ to 5+) for collision-induced dissociation fragmentation, with a cycle time of 3.3 s.

MS data were searched simultaneously against the *Mus musculus* Swissprot database (release 2018_01, 33,744 entries) and *P. berghei* Uniprot database (release 2016_07, 32,170 entries) with Mascot algorithm (version 2.5, Matrix Science), using the software's decoy strategy. Carbamidomethylation of cysteine was set as fixed modification; N-terminal protein acetylation, phosphorylation of serine/threonine/tyrosine, and oxidation of methionine were set as variable modifications; tryptic specificity with up to three miscleavages was used. The

mass tolerances in MS and MS/MS were set to 30 ppm and 0.5 Da respectively. The resulting .dat files were imported into Proline 2.0 software (https://www.profiproteomics.fr/proline/) (74) where they were validated with Mascot pretty rank equal to 1, 1% false discovery rate on both peptide spectrum matches, and protein sets (based on score). The total number of MS/MS fragmentation spectra was used to quantify each protein.

Sample (b) displayed only 143 (WT) and 170 (KO) proteins due to the strong lysis conditions caused by the presence of saponin and was thus discarded for bioinformatics analysis. For the statistical analysis of the data, we compared the spectral count data collected for tRip samples against the KO control with a negative-binomial test and calculated the fold change, a p value, and an adjusted p value for each identified protein. Exploratory data analysis revealed the presence of batch effects in our experiments, and the edgeR negative binomial general linear model regression was run with the following design: null model; y∼batch and alternative model; y∼treatment + batch. For this study, considered protein partners are statistically enriched in the tRip samples with an adjusted p value < 0.05 and a minimum log fold change of 2. The MS proteomics data have been deposited to the ProteomeXchange Consortium *via* the PRIDE (75) partner repository with the dataset identifier PXD033057 and 10.6019/PXD033057.

MS analysis of ERS-N, QRS-N, MRS-N, and tRip

As for coIP analysis, proteins were digested with trypsin before LC-MS/MS analysis. Generated peptides were separated either with a 250 min gradient on the NanoLC-2DPlus-TripleTOF 5600 system using the same column setup as for coIP or with a 60 min gradient on the Easy-nanoLC-1000 system equipped with a C18 analytical column (75 μm ID × 25 cm nanoViper, 3 μm Acclaim PepMap, Thermo Fisher Scientific) and coupled to the Q-Exactive Plus mass spectrometer (Thermo Fisher Scientific) operating in data-dependent acquisition mode with Xcalibur software (Thermo Fisher) using a "Top10" strategy.

Data were searched with Mascot algorithm (version 2.6, Matrix Science) on a combination of *Escherichia coli* sequences (Swissprot, *E. coli* K12, release 2022_01, 6507 entries) with contaminant proteins (release 2021_03, 111 entries) and the four sequences of interest. The mass tolerances in MS and MS/MS were set to 10 ppm and 0.02 Da, respectively. The resulting .dat files were imported into Proline 2.0 software where they were validated.

Bioinformatics

Protein sequences for tRip and cytosolic ERS, QRS, and MRS from all *Plasmodium* strains were retrieved from PlasmoDB (76). Related proteins from other organisms were searched using NCBI BLAST and relevant sequences were fetched from Uniprot (77). All MSAs were performed using T-coffee (https://tcoffee.crg.eu/) (78). LCRs in *Plasmodium* proteins were detected by aligning the sequences of different strains. Delimitation of additional sequences appended to *Plasmodium* aaRSs was achieved by alignment against prokaryotic homologs. HHpred (79) and Batch CDD search (80) were used to identify conserved domains in *Plasmodium* proteins by submitting either full-length sequences or specific segments. Secondary structure predictions were carried out with Quick 2D (81). Template-based 3D models of *P. berghei* proteins were generated using the Raptor X web server (48).

Plasmid constructions and production of recombinant proteins

Synthetic genes (GenScript) encoding *P. berghei* tRip and the GST-like domains of ERS, QRS, and MRS were cloned into pET15b. tRip was fused to an N-terminal 6His tag. The N-terminal domains of ERS, QRS, and MRS were fused either to a removable C-terminal 6His tag (removed by thrombin cleavage) or a removable SUMO-6His tag (removed by TEV cleavage). Besides improving solubility, addition of the SUMO peptide resulted in proteins of different sizes that could be distinguished by SDS-PAGE. Proteins with no tag were obtained by introducing a stop codon (TAA) before the thrombin site and mutations at specific amino acid positions were generated using the QuickChange site-directed mutagenesis kit (Agilent). Since the AT content of most *Plasmodium* protein genes is above 70% (82), sequences were optimized to increase expression of tRip and the three aaRSs. Sequences were adapted to human codon usage, even though the proteins were expressed in *E. coli*. In this way, the AT content was decreased, while some rare codons were retained to slow down translation of the recombinant protein in *E. coli*. All cultures were started from freshly transformed *E. coli* BL21(DE3) cells in LB medium supplemented with 100 μg/ml ampicillin. Cultures were inoculated to a starting A_{600nm} of 0.015 and incubated at 30 °C and 180 rpm until an A_{600nm} of 0.8 was reached. Protein expression was induced overnight at 16 °C with 0.5 mM isopropyl-β-D-thiogalactopyranoside. Induction of protein expression at low temperature (16 °C) was crucial to obtain soluble proteins. Expression and solubility of recombinant proteins were checked by SDS-PAGE.

In vitro *pull-down assays*

Interactions between tRip and the three other GST-like domains were investigated by *in vitro* pull-down assays. Bacteria expressing a 6His-tagged protein (bait) as well as one or more bacteria expressing untagged proteins (prey) were suspended in 1.2 ml binding buffer (50 mM Hepes–NaOH pH 8.0, 300 mM NaCl, 10% (v/v) glycerol, 20 mM imidazole, and 5 mM 2-mercaptoethanol [β-Me]) supplemented with 0.005% (w/v) n-dodecyl β-D-maltoside (DDM). Cells were disrupted by sonicating twice for 10 s at amplitude 40 (Vibracell 75022 UltraSonic Processor), and the crude extract was centrifuged at 15,000*g* for 15 min at 4 °C. The protein extract was incubated with 75 μl Ni-iminodiacetic acid agarose (Bio-Rad) for 30 min at room temperature on a tube rotator, and the mixture was transferred to an empty chromatography column (Sigma–Aldrich). The resin was washed twice with 2.5 ml of binding buffer with DDM and once

with 2.5 ml of binding buffer without DDM. Proteins specifically bound to the resin were eluted with 100 µl of binding buffer containing 250 mM imidazole. The protein contents of both the centrifuged extract and the eluate were analyzed by SDS-PAGE. To estimate the abundance of proteins in the eluate, the density of each band was quantified using Image J (https://imagej.nih.gov/ij/) (83). The value was divided by the number of arginine, lysine, and histidine residues to account for differences in Coomassie staining. Error bars were calculated from at least three replicates. Because the solubilities of WT and mutated proteins varied, the volumes of bacterial cultures were adapted to have similar amounts of each protein in the initial mixture.

Purification of complexes

Bacteria expressing individual recombinant proteins (one bait and several preys) were lysed together in lysis buffer (50 mM Hepes–NaOH pH 8.0, 300 mM NaCl, 10% (v/v) glycerol, 5 mM β-Me, and 0.005% (w/v) DDM). The volume was adapted so that 500 ml of culture was resuspended in 25 ml of lysis buffer. Each 25 ml sample was sonicated in ice for 7 min at 120 V (Annemasse Ultrasons apparatus) and ultracentrifuged at 45,000*g* for 45 min at 4 °C (Optima XE-90, Beckman-Coulter). The clarified extract was loaded onto a 1 ml Ni-NTA (His-Select HF, Sigma–Aldrich) column equilibrated with lysis buffer (BioLogic DuoFlow chromatography system). The column was washed with 15 ml of lysis buffer supplemented with 20 mM imidazole, 6 ml of a linear gradient (0.3–1.0 M NaCl) in the same buffer, 6 ml of the inverted gradient back to 0.3 M, and 33 ml of lysis buffer containing 20 mM imidazole. Retained proteins were eluted with 25 ml of lysis buffer containing 250 mM imidazole and the collected fractions for analysis by SDS-PAGE. Fractions were pooled and concentrated (Amicon ultrafiltration devices, Merck Millipore) and further analyzed on a SepFast 10/300 6 to 5000 kDa SEC column (BioToolomics) at 0.2 ml/min in SEC buffer (25 mM Hepes–NaOH pH 7.0, 300 mM NaCl, 5% (v/v) glycerol, 0.005% (w/v) DDM, and 5 mM β-Me). Fractions were analyzed on SDS-PAGE, and the abundance of each protein partner was estimated as described previously. Protein concentration was determined with a NanoDrop ND-1000 spectrophotometer (Thermo Fisher Scientific) and the A_{260}/A_{280} ratio was used to assess nucleic acid contamination ($A_{260}/A_{280} \approx 0.5$ for pure protein samples). SEC column was calibrated using either the MWGF1000 kit (Sigma–Aldrich) or the gel filtration standard (Bio-Rad). If removal of SUMO tags was required, proteins eluted from the Ni-NTA were dialyzed overnight at 4 °C against lysis buffer in the presence of TEV protease (6His-tagged, 1 µg of TEV per 25 µg of protein; homemade). The SUMO tag, 6His-TEV, and noncleaved complexes were eliminated by running the sample onto a second Ni-NTA column.

Light-scattering measurements

DLS and SLS measurements were performed with a Wyatt Technology DynaPro Nanostar instrument (100 mW He-Ne laser, λ = 658 nm, DLS θ = 90°, SLS θ = 90°, 500 channel correlator) using a 1 µl quartz cuvette (serial number JC-164) calibrated with toluene at 25 °C. Ten measurements, each one composed of 10 acquisitions of 5 s, were recorded at 20 °C and processed with DYNAMICS, version 7.8.1.3. (Wyatt Technology) Solvent refractive index and absolute viscosity were estimated using Malvern Panalytical DLS software, version 8, and the particle increment of refractive index (dn/dc) was assumed to be 0.185 ml/g. The intensity of the solvent alone (filtered through a membrane with a pore diameter of 0.1 µm) was measured and subtracted from the sample in SLS calculations. Several dilutions of freshly purified protein samples in SEC buffer were ultracentrifuged for 1 h at 100,000*g* at 4 °C (S45A rotor in Sorvall Hitachi Discovery M150E microultracentrifuge) before light-scattering measurements. Sample concentrations were verified using a NanoDrop ND-1000 spectrophotometer.

SEC-MALS experiments

SEC-MALS was performed at 25 °C using a Superose 6 10/300 GL column (GE Healthcare) attached to a light-scattering detector (miniDAWN TREOS, Wyatt Technology) and a differential refractive index detector (Optilab T-rEX, Wyatt Technology). The column was equilibrated with SEC buffer and detector normalization was achieved with bovine serum albumin (Sigma–Aldrich). Samples were ultracentrifuged 1 h at 100,000*g* at 4 °C before injection of Q-complex (30 µl at 6.8 mg/ml) or M-complex (50 µl at 8.6 mg/ml). Data were analyzed using ASTRA (Wyatt Technology), version 6.1.7.17.

EMSAs

Agarose gels

Protein complexes (3.3 µM) were incubated with increasing concentrations of total yeast tRNA (0.55–6.6 µM) in binding buffer (25 mM Hepes–NaOH pH 7.0, 150 mM NaCl, 10% (v/v) glycerol, 5 mM $MgCl_2$, 0.005% (w/v) DDM, and 5 mM β-Me), and 6.7 µM of dodeca-dT (competitor) for 20 min on ice. tRNA binding was analyzed by electrophoresis (75 V, 1 h 30 at 4 °C) on a 1% (w/v) low-melting agarose gel (Quantum Biotechnologies) in Tris–borate–EDTA buffer. Gels were first stained with ethidium bromide and then with InstantBlue Coomasie protein stain (Expedeon Ltd). Bands containing protein–RNA complexes were excised, melted at 95 °C, and mixed with one volume of 2X SDS-PAGE loading buffer. The pH was adjusted by adding a few microliters of concentrated NaOH, and samples were analyzed on 1.5 mm thick 12% SDS-PAGE.

Polyacrylamide affinity coelectrophoresis

Increasing concentrations of peptides (62.5 nM to 1 µM) were embedded in a 1.5 × 80 × 100 mm^3 6% (19/1) polyacrylamide gel. Samples (5 µl, 5 nM [3′-^{32}P] RNA in 25 mM Hepes–NaOH pH 7.0, 5 mM $MgCl_2$, 10% glycerol, and bromophenol blue) of radiolabeled total yeast tRNA were electrophoresed for 90 min 70 V at 4 °C. Gels were dried and analyzed on a Phosphor-Imager (Typhoon FLA 7000).

Data availability

All data files are available in the article and supplementary data. The mass spectrometry proteomics data are included in Table S1 and have been deposited to the ProteomeXchange

Consortium *via* the PRIDE partner repository with the dataset identifier PXD033057 and 10.6019/PXD033057.

Supporting information—This article contains supporting information.

Acknowledgments—We are grateful to Philippe Hammann, Lauriane Kuhn and Béatrice Chane Woon Ming for LC-MS/MS analysis, Pierre Poussin-Courmontagne for SEC-MALS experiments, and to Prof Tamara Hendrickson for providing comments on this article. This work was performed under the framework of the Interdisciplinary Thematic Institute IMCBio, as part of the ITI 2021 to 2028 program of the University of Strasbourg, CNRS and Inserm.

Author contributions—M. F. methodology; J. R. J. P., D. K., J. C, and C. P investigation; J. R. J. P. and M. F. data curation; M. F. and J. R. J. P. writing–original draft; M. F. and J. R. J. P. writing–review & editing; M. F. funding acquisition.

Funding and additional information—This work was performed under the framework of the Interdisciplinary Thematic Institute IMCBio, as part of the ITI 2021-2028 program of the University of Strasbourg, CNRS and Inserm. It was supported by IdEx Unistra (ANR-10-IDEX-0002), by SFRI-STRAT'US project (ANR 20-SFRI-0012), and EUR IMCBio (IMCBio ANR-17-EURE-0023) under the framework of the French Investments for the Future Program », by previous Labex NetRNA (ANR-10-LABX-0036), by the CNRS and the Université de Strasbourg, IdEx "Equipement mi-lourd" (2015), and CONACYT- Mexico (grant number 439648) to JRJP.

Conflict of interest—The authors declare that they have no conflicts of interest with the contents of this article.

Abbreviations—The abbreviations used are: β-Me, 2-mercaptoethanol; aaRS, aminoacyl-tRNA synthetase; AIMP, aaRS-interacting multifunctional protein; CDD, conserved domain database; coIP, coimmunoprecipitation; DDM, β-D-maltoside; DLS, dynamic light scattering; EMAPII, endothelial monocyte-activating polypeptide II; ERS, glutamyl-tRNA synthetase; EPRS, glutamyl–prolyl-tRNA synthetase; LCR, low-complexity region; MALS, multiangle light scattering; MRS, methionyl-tRNA synthetase; MS, mass spectrometry; MSA, multisequence alignment; MSC, multi-aaRS complex; MW, molecular weight; Ni-NTA, nickel-nitrilotriacetic acid; PDB, Protein Data Bank; QRS, glutaminyl-tRNA synthetase; SEC, size-exclusion chromatography; SLS, static light scattering; tRip, tRNA import protein.

References

1. Rubio Gomez, M. A., and Ibba, M. (2020) Aminoacyl-tRNA synthetases. *RNA* **26**, 910–936
2. Park, S. G., Ewalt, K. L., and Kim, S. (2005) Functional expansion of aminoacyl-tRNA synthetases and their interacting factors: New perspectives on housekeepers. *Trends Biochem. Sci.* **30**, 569–574
3. Pang, Y. L. J., Poruri, K., and Martinis, S. A. (2014) tRNA synthetase: tRNA aminoacylation and beyond. *Wiley Interdiscip. Rev. RNA* **5**, 461–480
4. Guo, M., and Schimmel, P. (2013) Essential nontranslational functions of tRNA synthetases. *Nat. Chem. Biol.* **9**, 145–153
5. Hyeon, D. Y., Kim, J. H., Ahn, T. J., Cho, Y., Hwang, D., and Kim, S. (2019) Evolution of the multi-tRNA synthetase complex and its role in cancer. *J. Biol. Chem.* **294**, 5340–5351
6. Han, J. M., Kim, J. Y., and Kim, S. (2003) Molecular network and functional implications of macromolecular tRNA synthetase complex. *Biochem. Biophys. Res. Commun.* **303**, 985–993
7. Lee, S. W., Cho, B. H., Park, S. G., and Kim, S. (2004) Aminoacyl-tRNA synthetase complexes: Beyond translation. *J. Cell Sci.* **117**, 3725–3734
8. Cui, H., Kapur, M., Diedrich, J. K., Yates, J. R., Ackerman, S. L., and Schimmel, P. (2021) Regulation of ex-translational activities is the primary function of the multi-tRNA synthetase complex. *Nucl. Acids Res.* **49**, 3603–3616
9. Guo, M., and Yang, X.-L. (2013) Architecture and metamorphosis. In aminoacyl-tRNA synthetases in biology and medicine. In Kim, S., ed., *Topics in Current Chemistry* **344**. Springer Netherlands, Dordrecht: 89–118
10. Havrylenko, S., and Mirande, M. (2015) Aminoacyl-tRNA synthetase complexes in evolution. *IJMS* **16**, 6571–6594
11. Karanasios, E., and Simos, G. (2010) Building arks for tRNA: Structure and function of the Arc1p family of non-catalytic tRNA-binding proteins. *FEBS Lett.* **584**, 3842–3849
12. Kapps, D., Cela, M., Théobald-Dietrich, A., Hendrickson, T., and Frugier, M. (2016) OB or Not OB: Idiosyncratic utilization of the tRNA-binding OB-fold domain in unicellular, pathogenic eukaryotes. *FEBS Lett.* **590**, 4180–4191
13. Simos, G., Segref, A., Fasiolo, F., Hellmuth, K., Shevchenko, A., Mann, M., *et al.* (1996) The yeast protein Arc1p binds to tRNA and functions as a cofactor for the methionyl- and glutamyl-tRNA synthetases. *EMBO J.* **15**, 5437–5448
14. van Rooyen, J. M., Murat, J.-B., Hammoudi, P.-M., Kieffer-Jaquinod, S., Coute, Y., Sharma, A., *et al.* (2014) Assembly of the novel five-component apicomplexan multi-aminoacyl-tRNA synthetase complex is driven by the hybrid scaffold protein tg-p43. *PLoS One* **9**, e89487
15. Cestari, I., Kalidas, S., Monnerat, S., Anupama, A., Phillips, M. A., and Stuart, K. (2013) A multiple aminoacyl-tRNA synthetase complex that enhances tRNA-aminoacylation in african trypanosomes. *Mol. Cell Biol.* **33**, 4872–4888
16. Ahn, H.-C., Kim, S., and Lee, B.-J. (2003) Solution structure and p43 binding of the p38 leucine zipper motif: coiled-coil interactions mediate the association between p38 and p43. *FEBS Lett.* **542**, 119–124
17. Havrylenko, S., Legouis, R., Negrutskii, B., and Mirande, M. (2011) Caenorhabditis elegans evolves a new architecture for the multi-aminoacyl-tRNA synthetase complex. *J. Biol. Chem.* **286**, 28476–28487
18. Negrutskii, B. S., and Deutscher, M. P. (1991) Channeling of aminoacyl-tRNA for protein synthesis *in vivo*. *Proc. Natl. Acad. Sci. U. S. A.* **88**, 4991–4995
19. Simos, G., Sauer, A., Fasiolo, F., and Hurt, E. C. (1998) A conserved domain within Arc1p delivers tRNA to aminoacyl-tRNA synthetases. *Mol. Cell* **1**, 235–242
20. Kyriacou, S. V., and Deutscher, M. P. (2008) An important role for the multienzyme aminoacyl-tRNA synthetase complex in mammalian translation and cell growth. *Mol. Cell* **29**, 419–427
21. Golinelli-Cohen, M.-P., and Mirande, M. (2007) Arc1p is required for cytoplasmic confinement of synthetases and tRNA. *Mol. Cell Biochem.* **300**, 47–59
22. Arif, A., Jia, J., Mukhopadhyay, R., Willard, B., Kinter, M., and Fox, P. L. (2009) Two-site phosphorylation of EPRS coordinates multimodal regulation of noncanonical translational control activity. *Mol. Cell* **35**, 164–180
23. Frechin, M., Enkler, L., Tetaud, E., Laporte, D., Senger, B., Blancard, C., *et al.* (2014) Expression of nuclear and mitochondrial genes encoding ATP synthase is synchronized by disassembly of a multisynthetase complex. *Mol. Cell* **56**, 763–776
24. Han, J. M., Lee, M. J., Park, S. G., Lee, S. H., Razin, E., Choi, E.-C., *et al.* (2006) Hierarchical network between the components of the multi-tRNA synthetase complex. *J. Biol. Chem.* **281**, 38663–38667
25. Laporte, D., Huot, J. L., Bader, G., Enkler, L., Senger, B., and Becker, H. D. (2014) Exploring the evolutionary diversity and assembly modes of multi-aminoacyl-tRNA synthetase complexes: Lessons from unicellular organisms. *FEBS Lett.* **588**, 4268–4278
26. Koonin, E. V., Tatusov, R. L., Altschul, S. F., Bryant, S. H., Mushegian, A. R., Bork, P., *et al.* (1994) Eukaryotic translation elongation factor 1γ contains a glutathione transferase domain-Study of a diverse, ancient

protein super family using motif search and structural modeling. *Protein Sci.* **3**, 2045–2055
27. Bec, G., Kerjan, P., and Waller, J. P. (1994) Reconstitution *in vitro* of the valyl-tRNA synthetase-elongation factor (EF) 1 beta gamma delta complex. essential roles of the NH2-terminal extension of valyl-tRNA synthetase and of the EF-1 delta subunit in complex formation. *J. Biol. Chem.* **269**, 2086–2092
28. Guo, M., Yang, X. L., and Schimmel, P. (2010) New functions of aminoacyl-tRNA synthetases beyond translation. *Nat. Rev. Mol. Cell Biol.* **11**, 668–674
29. Achilonu, I., Elebo, N., Hlabano, B., Owen, G. R., Papathanasopoulos, M., and Dirr, H. W. (2018) An update on the biophysical character of the human eukaryotic elongation factor 1 beta: Perspectives from interaction with elongation factor 1 gamma. *J. Mol. Recognit.* **31**, e2708
30. Koehler, C., Round, A., Simader, H., Suck, D., and Svergun, D. (2013) Quaternary structure of the yeast Arc1p-aminoacyl-tRNA synthetase complex in solution and its compaction upon binding of tRNAs. *Nucl. Acids Res.* **41**, 667–676
31. Kaminska, M., Havrylenko, S., Decottignies, P., Gillet, S., Maréchal, P. L., Negrutskii, B., *et al.* (2009) Dissection of the structural organization of the aminoacyl-tRNA synthetase complex. *J. Biol. Chem.* **284**, 6053–6060
32. Mirande, M. (2017) The aminoacyl-tRNA synthetase complex. In macromolecular protein complexes. In Harris, J. R., Marles-Wright, J., eds., *Subcellular Biochemistry* **83**. Springer International Publishing, Cham: 505–522
33. Khan, K., Baleanu-Gogonea, C., Willard, B., Gogonea, V., and Fox, P. L. (2020) 3-Dimensional architecture of the human multi-tRNA synthetase complex. *Nucl. Acids Res.* **48**, 8740–8754
34. Dirr, H., Reinemer, P., and Huber, R. (1994) X-ray crystal structures of cytosolic glutathione S-transferases. Implications for protein architecture, substrate recognition and catalytic function. *Eur. J. Biochem.* **220**, 645–661
35. Armstrong, R. N. (1997) Structure, catalytic mechanism, and evolution of the glutathione transferases. *Chem. Res. Toxicol.* **10**, 2–18
36. Aceto, A., Dragani, B., Melino, S., Allocati, N., Masulli, M., Ilio, C. D., *et al.* (1997) Identification of an N-capping box that affects the α6-helix propensity in glutathione S-transferase superfamily proteins: a role for an invariant aspartic residue. *Biochem. J.* **322**, 229–234
37. Cocco, R., Stenberg, G., Dragani, B., Principe, D. R., Paludi, D., Mannervik, B., *et al.* (2001) The folding and stability of human alpha class glutathione transferase A1-1 depend on distinct roles of a conserved N-capping box and hydrophobic staple motif. *J. Biol. Chem.* **276**, 32177–32183
38. Simader, H., Hothorn, M., Köhler, C., Basquin, J., Simos, G., and Suck, D. (2006) Structural basis of yeast aminoacyl-tRNA synthetase complex formation revealed by crystal structures of two binary sub-complexes. *Nucl. Acids Res.* **34**, 3968–3979
39. Karanasios, E., Simader, H., Panayotou, G., Suck, D., and Simos, G. (2007) Molecular determinants of the yeast arc1p–aminoacyl-tRNA synthetase complex assembly. *J. Mol. Biol.* **374**, 1077–1090
40. Hahn, H., Park, S. H., Kim, H.-J., Kim, S., and Han, B. W. (2019) The DRS–AIMP2–EPRS subcomplex acts as a pivot in the multi-tRNA synthetase complex. *IUCrJ* **6**, 958–967
41. Cho, H. Y., Lee, H. J., Choi, Y. S., Kim, D. K., Jin, K. S., Kim, S., *et al.* (2019) Symmetric assembly of a decameric subcomplex in human multi-tRNA synthetase complex *via* interactions between glutathione transferase-homology domains and aspartyl-tRNA synthetase. *J. Mol. Biol.* **431**, 4475–4496
42. Cho, H. Y., Maeng, S. J., Cho, H. J., Choi, Y. S., Chung, J. M., Lee, S., *et al.* (2015) Assembly of multi-tRNA synthetase complex *via* heterotetrameric glutathione transferase-homology domains. *J. Biol. Chem.* **290**, 29313–29328
43. Bour, T., Mahmoudi, N., Kapps, D., Thiberge, S., Bargieri, D., Ménard, R., *et al.* (2016) *Apicomplexa* -specific tRip facilitates import of exogenous tRNAs into malaria parasites. *Proc. Natl. Acad. Sci. U. S. A.* **113**, 4717–4722
44. Gupta, S., Chhibber-Goel, J., Sharma, M., Parvez, S., Harlos, K., Sharma, A., *et al.* (2020) Crystal structures of the two domains that constitute the Plasmodium vivax p43 protein. *Acta Crystallogr. D Struct. Biol.* **76**, 135–146
45. Frugier, M., Bour, T., Ayach, M., Santos, M. A., Rudinger-Thirion, J., Theobald-Dietrich, A., *et al.* (2010) Low Complexity Regions behave as tRNA sponges to help co-translational folding of plasmodial proteins. *FEBS Lett.* **584**, 448–454
46. Chaudhry, S. R., Lwin, N., Phelan, D., Escalante, A. A., and Battistuzzi, F. U. (2018) Comparative analysis of low complexity regions in Plasmodia. *Sci. Rep.* **8**, 335
47. Singh, G. P., Chandra, B. R., Bhattacharya, A., Akhouri, R. R., Singh, S. K., and Sharma, A. (2004) Hyper-expansion of asparagines correlates with an abundance of proteins with prion-like domains in Plasmodium falciparum. *Mol. Biochem. Parasitol.* **137**, 307–319
48. Källberg, M., Wang, H., Wang, S., Peng, J., Wang, Z., Lu, H., *et al.* (2012) Template-based protein structure modeling using the RaptorX web server. *Nat. Protoc.* **7**, 1511–1522
49. Frugier, M., Moulinier, L., and Giegé, R. (2000) A domain in the N-terminal extension of class IIb eukaryotic aminoacyl-tRNA synthetases is important for tRNA binding. *EMBO J.* **19**, 2371–2380
50. Francin, M., and Mirande, M. (2003) Functional dissection of the eukaryotic-specific tRNA-interacting factor of lysyl-tRNA synthetase. *J. Biol. Chem.* **278**, 1472–1479
51. Crepin, T., Peterson, F., Haertlein, M., Jensen, D., Wang, C., Cusack, S., *et al.* (2011) A hybrid structural model of the complete Brugia malayi cytoplasmic asparaginyl-tRNA synthetase. *J. Mol. Biol.* **405**, 1056–1069
52. Marchler-Bauer, A., Bo, Y., Han, L., He, J., Lanczycki, C. J., Lu, S., *et al.* (2017) CDD/SPARCLE: Functional classification of proteins *via* subfamily domain architectures. *Nucl. Acids Res.* **45**, D200–D203
53. Galani, K., Großhans, H., Deinert, K., Hurt, E. C., and Simos, G. (2001) The intracellular location of two aminoacyl-tRNA synthetases depends on complex formation with Arc1p. *EMBO J.* **20**, 6889–6898
54. Deinert, K., Fasiolo, F., Hurt, E. C., and Simos, G. (2001) Arc1p organizes the yeast aminoacyl-tRNA synthetase complex and stabilizes its interaction with the cognate tRNAs. *J. Biol. Chem.* **276**, 6000–6008
55. Quevillon, S., Agou, F., Robinson, J.-C., and Mirande, M. (1997) The p43 component of the mammalian multi-synthetase complex is likely to Be the precursor of the endothelial monocyte-activating polypeptide II cytokine. *J. Biol. Chem.* **272**, 32573–32579
56. Kaminska, M., Deniziak, M., Kerjan, P., Barciszewski, J., and Mirande, M. (2000) A recurrent general RNA binding domain appended to plant methionyl-tRNA synthetase acts as a cis-acting cofactor for aminoacylation. *EMBO J.* **19**, 6908–6917
57. Cahuzac, B. (2000) A recurrent RNA-binding domain is appended to eukaryotic aminoacyl-tRNA synthetases. *EMBO J.* **19**, 445–452
58. Cela, M., Théobald-Dietrich, A., Rudinger-Thirion, J., Wolff, P., Geslain, R., and Frugier, M. (2021) Identification of host tRNAs preferentially recognized by the *Plasmodium* surface protein tRip. *Nucl. Acids Res.* **49**, 10618–10629
59. Davies, H. M., Nofal, S. D., McLaughlin, E. J., and Osborne, A. R. (2017) Repetitive sequences in malaria parasite proteins. *FEMS Microbiol. Rev.* **41**, 923–940
60. Ko, Y.-G., Kang, Y.-S., Kim, E.-K., Park, S. G., and Kim, S. (2000) Nucleolar localization of human methionyl–trna synthetase and its role in ribosomal RNA synthesis. *J. Cell Biol.* **149**, 567–574
61. Hussain, T., Yogavel, M., and Sharma, A. (2015) Inhibition of protein synthesis and malaria parasite development by drug targeting of methionyl-tRNA synthetases. *Antimicrob. Agents Chemother.* **59**, 1856–1867
62. Mailu, B. M., Li, L., Arthur, J., Nelson, T. M., Ramasamy, G., Fritz-Wolf, K., *et al.* (2015) Plasmodium apicoplast gln-tRNAGln biosynthesis utilizes a unique GatAB amidotransferase essential for erythrocytic stage parasites. *J. Biol. Chem.* **290**, 29629–29641
63. Goodchild, S. C., Angstmann, C. N., Breit, S. N., Curmi, P. M. G., and Brown, L. J. (2011) Transmembrane extension and oligomerization of the CLIC1 chloride intracellular channel protein upon membrane interaction. *Biochemistry* **50**, 10887–10897
64. Hare, J. E., Goodchild, S. C., Breit, S. N., Curmi, P. M. G., and Brown, L. J. (2016) Interaction of human chloride intracellular channel protein 1

(CLIC1) with lipid bilayers: a fluorescence study. *Biochemistry* **55**, 3825–3833
65. Singh, H. (2010) Two decades with dimorphic chloride intracellular channels (CLICs). *FEBS Lett.* **584**, 2112–2121
66. Argenzio, E., and Moolenaar, W. H. (2016) Emerging biological roles of Cl– intracellular channel proteins. *J. Cell Sci.* **129**, 4165–4174
67. Minns, A. M., Hart, K. J., Subramanian, S., Hafenstein, S., and Lindner, S. E. (2018) Nuclear, cytosolic, and surface-localized poly(A)-Binding proteins of Plasmodium yoelii. *mSphere* **3**, e00435-17
68. Lindner, S. E., Swearingen, K. E., Harupa, A., Vaughan, A. M., Sinnis, P., Moritz, R. L., *et al.* (2013) Total and putative surface proteomics of malaria parasite salivary gland sporozoites. *Mol. Cell Proteomics* **12**, 1127–1143
69. Cha, S.-J., Kim, M.-S., Pandey, A., and Jacobs-Lorena, M. (2016) Identification of GAPDH on the surface of Plasmodium sporozoites as a new candidate for targeting malaria liver invasion. *J. Exp. Med.* **213**, 2099–2112
70. White, M. R., and Garcin, E. D. (2016) The sweet side of RNA regulation: glyceraldehyde-3-phosphate dehydrogenase as a noncanonical RNA-binding protein: The sweet side of RNA regulation. *WIREs RNA* **7**, 53–70
71. Jones, M. L., Kitson, E. L., and Rayner, J. C. (2006) Plasmodium falciparum erythrocyte invasion: A conserved myosin associated complex. *Mol. Biochem. Parasitol.* **147**, 74–84
72. Goel, V. K., Li, X., Chen, H., Liu, S.-C., Chishti, A. H., and Oh, S. S. (2003) Band 3 is a host receptor binding merozoite surface protein 1 during the Plasmodium falciparum invasion of erythrocytes. *Proc. Natl. Acad. Sci. U. S. A.* **100**, 5164–5169
73. Lange, H., Ndecky, S. Y. A., Gomez-Diaz, C., Pflieger, D., Butel, N., Zumsteg, J., *et al.* (2019) RST1 and RIPR connect the cytosolic RNA exosome to the Ski complex in Arabidopsis. *Nat. Commun.* **10**, 3871–3882
74. Bouyssié, D., Hesse, A.-M., Mouton-Barbosa, E., Rompais, M., Macron, C., Carapito, C., *et al.* (2020) Proline: an efficient and user-friendly software suite for large-scale proteomics. *Bioinformatics* **36**, 3148–3155
75. Perez-Riverol, Y., Bai, J., Bandla, C., García-Seisdedos, D., Hewapathirana, S., Kamatchinathan, S., *et al.* (2022) The PRIDE database resources in 2022: a hub for mass spectrometry-based proteomics evidences. *Nucl. Acids Res.* **50**, D543–D552
76. PlasmoDB. (2001) An integrative database of the Plasmodium falciparum genome. Tools for accessing and analyzing finished and unfinished sequence data. *Nucl. Acids Res.* **29**, 66–69
77. The UniProt Consortium, Bateman, A., Martin, M.-J., Orchard, S., Magrane, M., Agivetova, R., Ahmad, S., *et al.* (2021) UniProt: The universal protein knowledgebase in 2021. *Nucl. Acids Res.* **49**, D480–D489
78. Magis, C., Taly, J.-F., Bussotti, G., Chang, J.-M., Di Tommaso, P., Erb, I., *et al.* (2014) T-Coffee: tree-based consistency objective function for alignment evaluation. In multiple sequence alignment methods. In Russell, D. J., ed., *Methods in Molecular Biology* **1079**. Humana Press, Totowa, NJ: 117–129
79. Soding, J., Biegert, A., and Lupas, A. N. (2005) The HHpred interactive server for protein homology detection and structure prediction. *Nucl. Acids Res.* **33**, W244–W248
80. Marchler-Bauer, A., Derbyshire, M. K., Gonzales, N. R., Lu, S., Chitsaz, F., Geer, L. Y., *et al.* (2015) Cdd: NCBI's conserved domain database. *Nucl. Acids Res.* **43**, D222–D226
81. Zimmermann, L., Stephens, A., Nam, S.-Z., Rau, D., Kübler, J., Lozajic, M., *et al.* (2018) A completely reimplemented MPI bioinformatics toolkit with a new HHpred server at its core. *J. Mol. Biol.* **430**, 2237–2243
82. Gardner, M. J., Hall, N., Fung, E., White, O., Berriman, M., Hyman, R. W., *et al.* (2002) Genome sequence of the human malaria parasite *Plasmodium falciparum*. *Nature* **419**, 498–511
83. Abràmoff, M.,D., Magalhães, P.,J., and Ram, S.,J. (2004) Image processing with ImageJ. *Biophot. Int.* **11**, 36–42
84. Robinson, J.-C., Kerjan, P., and Mirande, M. (2000) Macromolecular assemblage of aminoacyl-tRNA synthetases: quantitative analysis of protein-protein interactions and mechanism of complex assembly. *J. Mol. Biol.* **304**, 983–994